



Expert statement

Prothioconazole is chemically not a triazole, it is a triazolinethione, and thus does not cause the developmental and reproductive toxicity observed for several classical triazoles

Authors:

[REDACTED]

[REDACTED]

**Bayer AG
Crop Science Division
Alfred-Nobel-Str. 50
40789 Monheim / Rhein
GERMANY**

Date: May 18, 2018



M-624093-01-2

OWNERSHIP STATEMENT

This document, the data contained in it and copyright therein are owned by Bayer AG. No part of the document or any information contained therein may be disclosed to any third party without the prior written authorisation of Bayer AG.



Contents

1) Introduction and executive summary	3
2) Mode of action of azole developmental and reproductive toxicity.....	6
3) Prothioconazole (PTZ) is chemically and toxicologically not a triazole.....	7
4) New computational chemistry data demonstrate a very weak and atypical binding mode of PTZ to CYP450 enzymes	8
A) Outline of this section.....	8
B) The binding of PTZ and PTZ-desthio to CYP51 differs fundamentally, in strength as well as in mode of binding.	9
C) Quantum Chemical Calculations not only confirm type II binding of PTZ-desthio, but also provide an explanation for the weak, non-type II binding mode of PTZ.....	11
D) Review of previous theoretical work on CYPs.....	13
E) Outline of the calculation procedure.....	13
F) Validation of the computational procedure by comparing calculation results with experimental data available for PTZ-desthio binding to CYP51	16
G) Binding modes of PTZ and PTZ-desthio are fundamentally different, with respect to Geometry, Topology as well as Binding Strength	17
i) The 3D binding-pose of the PTZ-headgroup to heme differs significantly from that of triazoles, while PTZ-desthio's triazole moiety shows the triazole-typical binding pose. ...	18
ii) Analysis of the electron densities shows that also the electronic modes of binding of PTZ and PTZ-desthio differ significantly	20
iii) In terms of binding enthalpy, PTZ-desthio binds significantly more strongly to CYP51 than PTZ.....	23
H) Summary of the quantum chemical calculations	25
I) Based on the CYP51 findings, conclusion by analogy allows similar trends to be expected for CYP19 and CYP26	26
J) Theoretical conclusions match experimental evidence	28
5) The unique metabolic detoxification principle of PTZ in humans and mammals	30
6) References	32



1) Introduction and executive summary

This summary is an extract of the more detailed sections 2) to 5) of this document which include respective references and further explanations to the figures.

The fungicide prothioconazole (PTZ) is important for controlling disease and protecting yield in various crops, particularly in cereals. It is also one of the key tools for reducing levels of mycotoxins in cereal and maize food and feed. Mycotoxins are naturally-occurring, highly toxic substances produced by certain fungal pathogens that can induce human illness.

At the molecular level, the antifungal activity of PTZ and triazoles in general is due to their ability to inhibit CYP51. This enzyme is essential for building of fungal cell membranes and thus survival of the fungus. CYP51 is a member of the cytochrome P450 superfamily of enzymes and inhibition of CYP enzymes by triazoles is not necessarily restricted to CYP51. Of particular relevance is the fact that mammalian CYP19 (aromatase), the enzyme essential for the end stages of conversion of androgens to oestrogens, can also be affected, as can the mammalian CYP26 family of enzymes involved in catabolism of the endogenous morphogen, retinoic acid.

Reproductive toxicity testing of several classical triazoles revealed late foetal deaths in mammals (likely a consequence of CYP19 inhibition), and teratogenicity (mainly cleft palate and limb malformations - possibly a consequence of CYP26 inhibition and resulting imbalance of retinoic acid equilibrium).

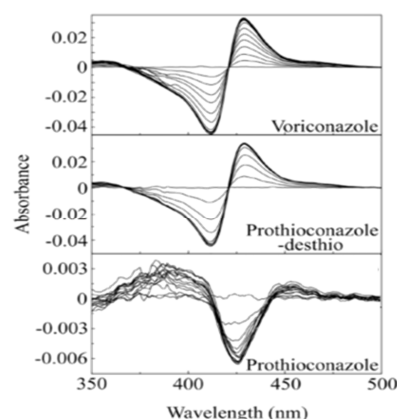
Over recent years, several of the classical triazole fungicides have been classified as reproductive toxic Cat 1B ("cut off" classification) by ECHA.

In contrast, PTZ is chemically not a triazole, but a triazolinethione, and does not cause the aforementioned reproductive and developmental toxicity associated with classical triazoles. PTZ should, therefore, not be classified as toxic for reproduction.

Following recent authority feedback, Bayer AG realized that it is important to convincingly demonstrate **the reason WHY prothioconazole does not cause the reproductive toxicity associated with triazoles.**

It was hypothesized that the structural difference between PTZ (a triazolinethione) and classical triazoles could lead to different ways of interaction with CYP450 enzymes, including the mammalian CYP19 and CYP26. Indeed, it has been shown that PTZ does not inhibit CYP19.

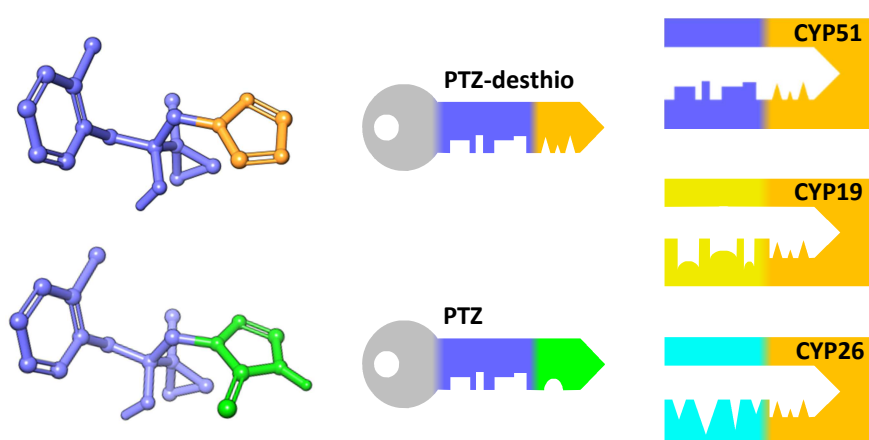
The binding mode to the heme ferric ion in the active site of the enzyme has a strong influence on the inhibition of the enzyme. **Published UV spectroscopic results** (see adjacent absorbance difference spectra of the progressive titration of *Candida albicans* CaCYP51 with different ligands) and crystallographic data indicate that any putative interaction of PTZ with the heme ferric ion of fungal and human CYP51 must be fundamentally different from the very typical interactions with heme commonly observed for classical triazoles.





However, the electronic nature of binding of PTZ to CYP enzymes was as yet unknown. Therefore **Bayer AG recently generated conclusive quantum computational chemistry data** for PTZ and, as a model for a classical triazole, also for the metabolite PTZ-desthio which has a triazole moiety. These data are presented here for the first time and provide solid atomistic reasoning as to why PTZ exhibits a very weak and atypical binding mode to CYP450 enzymes. Specifically, the binding mode of PTZ is fundamentally different to that of triazoles with respect to geometry, topology as well as binding strength.

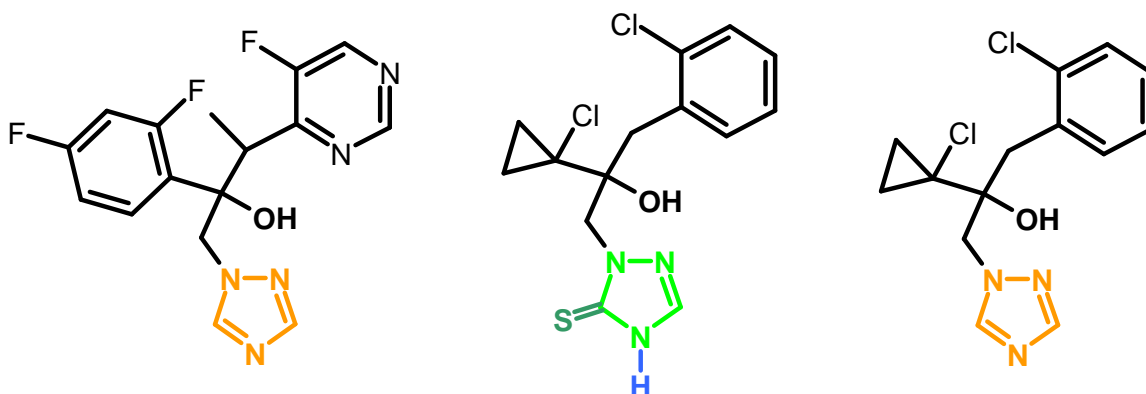
Translating the complex new quantum chemistry results into a simplistic “key-and-lock” picture should make the new findings intuitively understandable:



The metabolite PTZ-desthio has the classical triazole head which binds strongly to the heme ferric ion in the active site of the different CYP enzymes (see above; both the triazole head of the ligand as well as the heme in the active sites of the enzymes are marked with orange color). In contrast, PTZ’s triazolinethione head (marked in green) binds only very weakly and atypically to the heme in any CYP enzyme (and, thus, does not cause the reproductive toxicity associated with classical triazoles). The “body” of the keys (marked in blue) is identical for both PTZ and PTZ-desthio and may modulate for PTZ-desthio (and classical triazole fungicides) the generally strong binding affinity to the different CYP enzymes (due to differences in the active site channels - the “bodies of the locks”).

Furthermore, the already previously available Bayer AG proprietary animal and human metabolism data (“*unique principle of metabolic detoxification*” – see next page) complete the reasoning as to why PTZ does not cause the reproductive toxicity associated with classical triazoles and why PTZ has a generally very low toxicity in mammals.

Overall, the basis for the beneficial toxicological profile of the triazolinethione PTZ, compared to classical triazoles and the metabolite PTZ-desthio, can be “visually summarized” as follows:



The structural comparison of a classical triazole (left: voriconazole; the triazole head-group is highlighted in **orange** color) and PTZ (a triazolinetione; middle) reveals chemical differences which are marked for PTZ in **light-green + dark-green + blue** color. The metabolite PTZ-desthio (right) has a classical triazole moiety.

The **sulphur (S)** and the **hydrogen (H)** atoms in the 5-membered ring are unique to PTZ and contribute, via different mechanisms, to the **absence of triazole-related reproductive toxicity** and the **general low toxicity of PTZ** as follows:

- **Absence of classical triazole CYP450 binding/inhibition:** The hydrogen atom prevents a tight binding of the nitrogen to the heme in the active site of CYP450 enzymes.
 - **However, very weak and atypical binding to CYP450 enzymes can still occur via the sulfur atom.**
- **“Unique metabolic principle of detoxification” (excretion):** The sulfur atom functions as a “handle” for glucuronic acid, a highly efficient detoxification agent present in mammals, including humans. In the liver, this leads to the formation of the metabolite PTZ-S-glucuronide, which is rapidly excreted via bile and urine.
- **After glucuronic acid conjugation, the S is protected against cleavage and only a negligible amount of PTZ-desthio is systemically found in rats.** This “detoxification” principle has also been recently verified in human liver cells.

Overall it can be concluded that the available data base, including the newly-generated quantum computational chemistry data, provides a scientifically sound explanation as to why PTZ does not cause the reproductive toxicity associated with classical triazoles. Thus, PTZ should not be classified as toxic for reproduction.



2) Mode of action of azole developmental and reproductive toxicity

Azoles were first developed in the 1970s for use as anti-fungal agents in agriculture and also as therapeutic agents to treat human and animal fungal infections¹.

The antifungal activity of azole compounds is due to their ability to inhibit 14- α demethylase (CYP51), the enzyme responsible for a key step in the conversion of lanosterol or eburicol to finally ergosterol and/or fungisterol, steroids constitutive of fungal cell membranes².

CYP51 is a member of the cytochrome P450 superfamily of enzymes and inhibition of CYP enzymes by azole compounds is not restricted to CYP51. Of particular relevance is the fact that aromatase (CYP19), the enzyme essential for the end stages of conversion of androgens to oestrogens, can also be affected³, as can the CYP26 family of enzymes involved in catabolism of retinoic acid⁴.

As for all new chemicals and drugs, azoles have been subjected to comprehensive programmes of toxicity testing, including reproductive toxicity investigations. Embryofoetal developmental toxicity studies in rodents have highlighted two findings associated with maternal treatment with some but not all azoles. The first finding is a consequence of aromatase inhibition, which results in depletion of maternal oestrogen levels. In studies where the dosing period has been continued to at least gestation day (GD) 16 a marked increase in late foetal deaths has been recorded^{5,6,7,8}. Rey Moreno et al.⁹ demonstrated that, for epoxiconazole, the late deaths were associated with placental degeneration. Co-administration of oestrogen ameliorated the placental damage⁹ and reduced the incidence of late deaths^{10,8}. The second finding is teratogenicity at maternally toxic doses with a number of azoles, including epoxiconazole⁸, fluconazole¹¹, itraconazole¹², ketoconazole^{13,14}, triadimefon¹⁵ and voriconazole¹⁶. The spectrum of abnormalities reported in rats and/or mice has included craniofacial abnormalities, cleft palate, limb and/or axial skeletal defects. Additionally, a number of azoles have been suspected of being teratogenic in humans, for example fluconazole^{11,17} and voriconazole¹⁶. It has been suggested that inhibition of CYP26 might be a causative factor involved in azole teratogenicity, since CYP26 is essential for the catabolism of the endogenous morphogen, retinoic acid^{18,19}. The retinoic acid pathway has the crucial role of regulating the spatiotemporal balance of retinoic acid in the developing embryo, supporting normal growth and differentiation. Administration of retinoic acid to rats or mice can result in the development of abnormalities very similar to those reported above. Interference with retinoic acid catabolism could lead to an accumulation of retinoic acid in the embryonic tissues and thus give rise to abnormalities.



3) Prothioconazole (PTZ) is chemically and toxicologically not a triazole

Chemically PTZ is not a triazole (with an unsubstituted triazole ring), but a triazolinethione (see Figure 1).

The chemical structure has been confirmed by the physical methods NMR spectroscopy and crystallography²⁰.

Guideline developmental and reproductive toxicity studies with PTZ conducted in rats and rabbits did not show the typical triazole effects, described above²¹. This suggests that the structural difference between the PTZ molecule (a triazolinethione) and other classical triazoles could explain the difference in the interaction with CYP450 enzymes, including the mammalian CYP19 and CYP26.

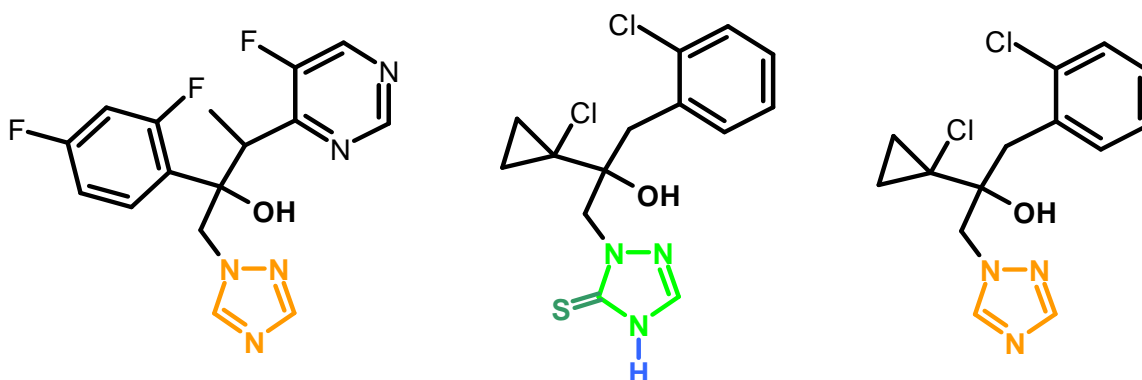


Figure 1: Structural comparison of triazole and triazolinethione moieties

Structural comparison of a classical triazole (left: voriconazole; the triazole head-group is highlighted in orange color) and PTZ (a triazolinethione; middle). The chemical difference in PTZ is highlighted by light-green + dark-green + blue color. The Sulphur (S) and the hydrogen (H) atoms in the 5-membered ring are unique to PTZ and constitute, via different mechanisms, the absence of triazole-related reproductive toxicity and the general low toxicity of PTZ. The metabolite PTZ-desthio (right) has a classical triazole moiety.

This hypothesis is supported by the findings of Kjeldsen et al.²² who have shown that PTZ does not inhibit aromatase (CYP19) in a human choriocarcinoma cell line.

No experimental data are available for the interaction of PTZ with the CYP26 enzyme. However, Parker et al.²³ demonstrated that the mechanism of binding of PTZ to the fungal *Mycosphaerella graminicola* (Mg) CYP51 differs from that of other azole antifungals. PTZ bound to MgCYP51 with 840-fold less affinity than epoxiconazole and, unlike several classical azoles, which are noncompetitive inhibitors, PTZ was found to be a competitive inhibitor of substrate binding. This is supported by Warrilow et al.²⁴ who showed that PTZ bound with up to 610-fold less affinity to *Candida albicans* CYP51 compared with other agricultural and medicinal azoles. PTZ also had the lowest binding affinity to human CYP51 and the least potency to inhibit fungal and human CYP51 enzyme activity. Based on the analyses of the spectral properties, both publications came to the conclusion that in contrast to the classical azoles, "PTZ does not coordinate directly with the heme ferric ion" of fungal and human CYP51.



Furthermore, the very favourable toxicological profile of PTZ is also supported by the published results of two already validated *in vitro* tests for studying the developmental toxicity of xenobiotics. PTZ showed the lowest embryotoxic potential in the rat whole embryo culture (WEC) assay²⁵ and the least potency to inhibit the differentiation of embryonic stem cells (EST)²⁶ among 12 tested azoles. To elucidate the underlying cause for the potency differences of the tested azoles to disturb embryonic development, transcriptomic analyses were performed in both *in vitro* test systems. The analysis revealed that most of the azoles investigated changed the expression of genes in the sterol biosynthesis pathway and embryonic developmental genes, dominated by genes in the retinoic acid pathway. As mentioned above, perturbations in the retinoic acid pathway are considered a causative factor involved in azole teratogenicity. In contrast to most of the other tested azoles, PTZ only slightly affected the transcription of genes involved in the embryonic pathways under investigation^{26,27}.

4) New computational chemistry data demonstrate a very weak and atypical binding mode of PTZ to CYP450 enzymes

A) Outline of this section

The section starts with a review of experimental (biochemical and spectroscopic) evidence that PTZ's binding to CYP51 is inherently different from that of classical triazoles. The mode of binding of PTZ-desthio, a major PTZ metabolite^{28,29} with a triazole moiety, to yeast CYP51 was elucidated by spectroscopy³⁰ and X-ray crystallography³¹. These experimental findings provide the starting point for in depth quantum chemical calculations, in which the binding mode of PTZ-desthio is explained in electronic detail. The electronic nature of binding for PTZ has not been investigated before; the theoretical calculations presented here for the first time provide a solid hypothesis on the binding mode of PTZ. In summary, these calculations provide atomistic reasoning as to why

- i. the modes of binding of PTZ and PTZ-desthio to CYP51 differ fundamentally,
- ii. the affinity of PTZ-desthio to CPY51 is high, while the affinity of PTZ is weak,

in agreement with the biochemical and spectroscopic findings.

Most of the section is devoted to the interaction of PTZ-desthio and PTZ as ligands of yeast CYP51; in a final paragraph, the 3D architecture of the yeast CYP51 protein itself is compared with human CYP19 and CYP26, and conclusions of analogy are derived, explaining why

- iii. the low affinity of PTZ to CYP51 translates into low affinity to other CYP enzymes.

Short introductions into concepts are provided by short paragraphs entitled "intermezzo". Readers may safely skip these paragraphs without missing the line of argument.



B) The binding of PTZ and PTZ-desthio to CYP51 differs fundamentally, in strength as well as in mode of binding.

As shortly described in the preceding section, scientists from Swansea University, Rothamsted Research and Texas Tech University characterized binding of PTZ to *Mycosphaerella graminicola* CYP51 (MgCYP51) and to *Candida albicans* CYP51 (CaCYP51) in 2011²³ and 2013³⁰ to investigate the *in vitro* activity of PTZ and PTZ-desthio. PTZ-desthio binds tightly to both CYP51s, producing strong prototypical difference spectra indicative of a triazole-bound low-spin CYP51 complex (so called “type II”-binding, see Figure 2, panels a and b). This confirms binding via direct coordination of the triazole N-4 as the sixth ligand of the heme ferric ion. In contrast, PTZ binds only weakly to MgCYP51 or CaCYP51. Moreover, PTZ’s difference spectra show a fundamentally different behaviour compared to the type II binders. PTZ’s weak so-called “type I” binding-mode is usually associated with substrate-, not inhibitor-binding.

The affinity of PTZ and PTZ-desthio to fungal versus human CYP51 was investigated as well, showing that PTZ binds weakly not only to fungal CaCYP51, but also to the human homolog $\Delta 60\text{HsCYP51}$. The affinity of PTZ to human CYP51 is so low that an IC₅₀ value for the inhibition of $\Delta 60\text{HsCYP51}$ enzyme activity could not be determined. (Ref.²⁴, Table 1).

Table 1: Equilibrium constants (K_d) for the formation of the protein-ligand complex, as well as observed 50% inhibitory concentrations (IC₅₀) for PTZ and PTZ-desthio with respect to fungal and human CYP51

Note that for PTZ an IC₅₀ could not be established for human CYP51, because no significant inhibition occurred in presence of up to 290 μM PTZ. The outer right column provides the type of difference spectra. Smaller K_d values correspond to higher affinity and stronger binding at molecular level. Small IC₅₀ are indicative of strong biochemical effect (Ref.²⁴).

	IC_{50} (μM)		K_d (nM)		spectroscopy
	CaCYP51	$\Delta 60\text{HsCYP51}$	CaCYP52	$\Delta 60\text{HsCYP52}$	
PTZ	150	none	6100	910	Type I
PTZ-desthio	0.6	100	41	39	Type II

The type II binding mode of PTZ-desthio, i.e. by direct coordination of the triazole to the heme-iron, was proven only recently by X-ray crystallographic elucidation of co-crystals of PTZ-desthio with Yeast CYP51 (Ref.³¹). Figure 2c shows that PTZ-desthio indeed binds to the heme-iron as suggested by the spectroscopic data. The authors were able to derive X-ray structures for the respective complexes with several classical triazoles. When overlaying these structures, the type II binding of all of them is obvious, with the N-4 of the triazole/imidazole head complexing the heme-iron in a centro-symmetrical fashion. As a remarkable side observation, the positions of active site amino acid residues do not significantly vary between these very different ligands. This fact will become important later, when we derive an atomistic binding mode hypothesis for PTZ.

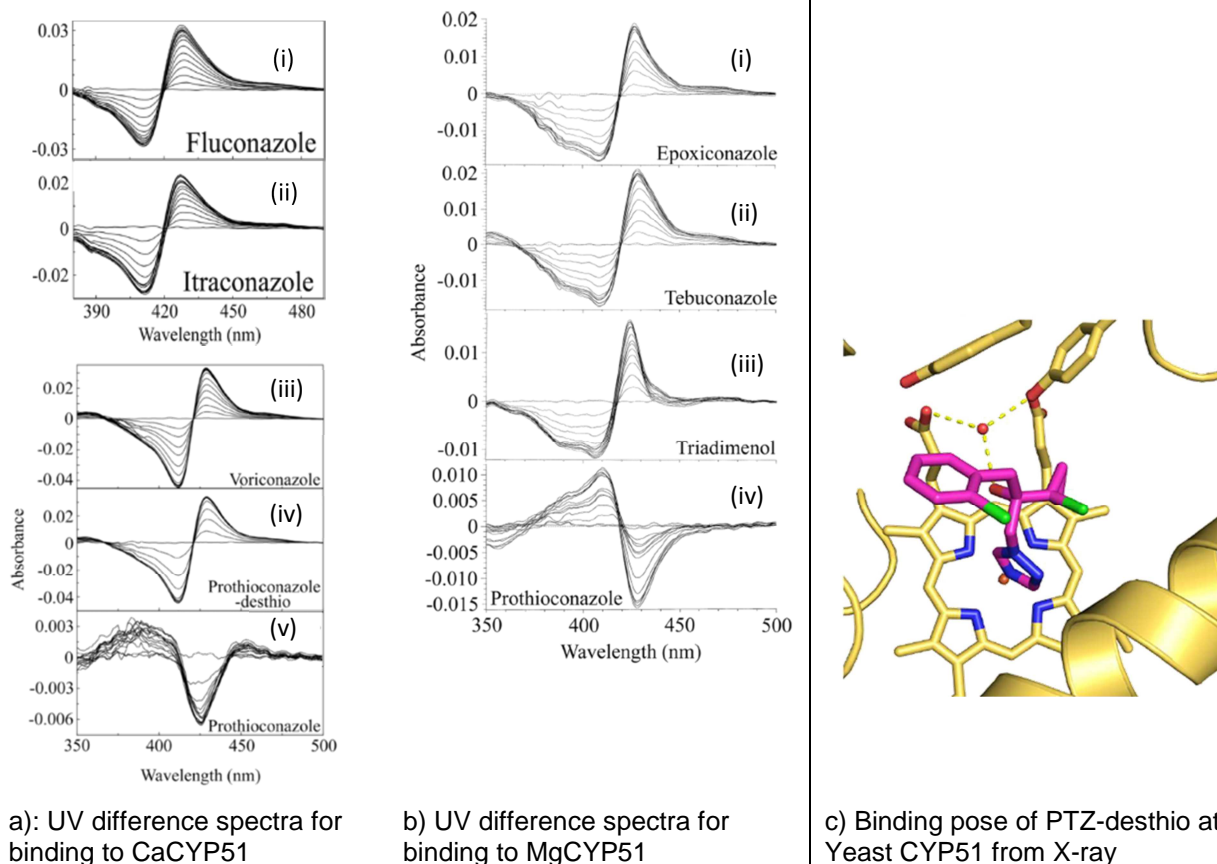


Figure 2: Spectroscopic data and crystallographic visualization of the binding mode

Panel a): Absorbance difference spectra for progressive titration of *Candida albicans* CaCYP51 with classical triazoles; fluconazole (i), itraconazole (ii), voriconazole (iii), PTZ-desthio (iv) in contrast to PTZ (v) (i and ii adapted from Ref.²⁴, iii to v adapted from Ref.³⁰). Panel b): Absorbance difference spectra for progressive titration of *Mycosphaerella graminicola* MgCYP51 with classical triazoles; epoxiconazole (i), tebuconazole (ii), triadimenol (iii), again in contrast to PTZ (iv) (Adapted from Ref.²³). **For all azole-like binders, note the uniformity of the prototypical, so-called “type II” shapes of spectra, in contrast to the “type I”-shape for PTZ in panels a(v) and b(iv).**

Panel c): PTZ-desthio complexed in the active site of Yeast CYP51 (PDB ID³²:5EAD). The ligand is shown with magenta carbons. The heme cofactor and selected residues (two tyrosines, as well as an interacting water molecule) are shown as sticks with yellow carbons. Adapted from Ref.³¹.

As stated previously, the X-ray data in Ref.³¹ were obtained using *S. cerevisiae* lanosterol 14 α -demethylase. Comparison with CYP51 structures from fungal pathogens including *Candida albicans*, *Candida glabrata* and *Aspergillus fumigatus* provides strong evidence for a highly conserved CYP51 structure including the drug binding site. Thus the basic findings should be transferable between these species.

No co-crystals are available for PTZ itself, thus experimental evidence on the atomistic detail on how PTZ binds to CYPs is missing.

C) Quantum Chemical Calculations not only confirm type II binding of PTZ-desthio, but also provide an explanation for the weak, non-type II binding mode of PTZ

1st Intermezzo: Classical versus Quantum Mechanics.

This paragraph may be skipped by readers with a theoretical or physical chemistry background.



Figure 3: Classical view of a molecule

The H₂-molecule as an object of classical mechanics: Two masses connected by a spring.

When using the term “classical mechanics” one essentially refers to the work of Isaac Newton, with the famous equation $\vec{F} = m \vec{a}$, force = mass times acceleration. In such a classical picture, molecules consist of small masses which are connected by forces, very much like a model built out of small wooden spheres connected by elastic springs. The force-constants of the springs and the angles between them determine the 3D shape of a molecule. This picture, often referred to as “force-field approach” may sound naive, but it is surprisingly successful in many areas of molecular modelling. Since the advent of quantum theory more than 100 years ago, we know that classical mechanics does not apply at the molecular, atomic and sub-atomic scales. This is the reign of quantum theory, a seemingly weird, but definitely counter-intuitive theory. Einstein, for example, did not like it at first, due to its strange behavior. However, the mathematical predictions based on quantum theory have been put to countless tests over the last century, and have withstood them all. And some of Einstein’s most weirdest predictions could finally be experimentally confirmed³³.

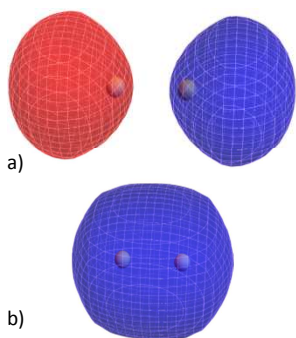


Figure 4: Quantum view of a molecule

The H₂-molecule as an object of quantum mechanics showing an “anti-bonding state” (a) and a “bonding state” (b). The spheres indicate the two nuclei of the molecule.

The central equation of quantum theory is the Schrödinger equation, $\hat{H}|\psi\rangle = E|\psi\rangle$, where E is the energy and Ψ is an abstract object called the “wave function”. The Hamiltonian operator \hat{H} is a mathematical description of the molecule. When solving the Schrödinger equation, one obtains two immediate results, the energy and the wave function. While the energy is directly observable, the wave function is not. However, with the help of the wave function, many observable properties of a system can be calculated, as set forth in the following. The application of quantum theory to molecules is called “quantum chemistry”, and properties which can be calculated include the 3D shape of a molecule, its energy, dipole moment, interactions with other molecules, etc. The problem is that the Schrödinger equation can be exactly solved only for very simple systems, like the H₂⁺-molecule. Fortunately, clever approximations such as the “Density Functional Theory (DFT)” allow application of the theory to large molecules³⁴. The advantage of Quantum Chemistry over Force Field methods lies in the fact that no prior knowledge about a molecule is needed: We don’t have to decide, which spheres (atoms) we have to connect with which kind of springs (forces). All derives from the wave function. The price to pay is that the computational cost of quantum chemical calculations is often far higher than that of classical approaches.



2nd Intermezzo: Quantum Theory level of theory is needed, as classical mechanics is likely to fail in the case of CYP-binding.

This paragraph may be skipped by readers experienced in computational chemistry.

One may argue that quantum theory is only rarely applied to protein ligand complexes, and may be considered “over-done”. By far most computational studies today employ heuristic schemes (“docking”) or are based on classical mechanics (“force-fields”, including “Free Energy Perturbation” approaches). These methods have a proven record³⁵, especially in “virtual screening”, meaning performing in-silico experiments with thousands or millions of ligands. But for the current case, these methods are not appropriate. First, in a virtual screening experiment, the accuracy of an **individual** calculation is not so critical. The calculations are deemed successful, as long as they deliver results which are far better than a random selection experiment. In our case, however, we are looking at just one protein-ligand complex and cannot hope for the law of high numbers to rescue our in silico experiment. Moreover, CYP51 contains a heme with a central Fe-atom. The electronic structure of the heme is rather complex, see Figure 5, with the many possible so-called “spin couplings” in the central iron atom adding to the complexity. Electron spin is not a classical property, but arises only in quantum mechanics (electron spin is sometimes described as the “angular momentum” of the electron, but this is not correct). Such situations are notoriously overwhelming for even the most advanced classical Force Fields. In addition, we will be looking for yet unknown modes of binding of PTZ at CYP51, and would like to do so as objectively as possible.

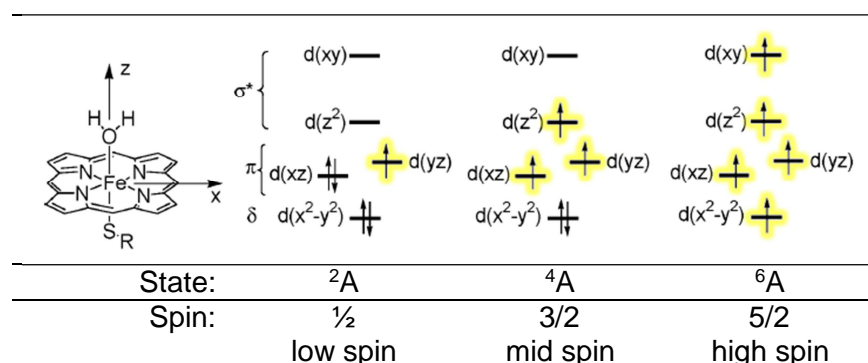


Figure 5: Spin states of Fe³⁺ in the resting state of P450_{cam} (CYP101)

The diagrams on the right symbolize the relevant “orbitals” (horizontal lines) which host, in our case, five electrons (vertical arrows). Each line/orbital can host a maximum of two electrons. Two electrons in an electron pair occupying one orbital must have opposite spins. Unpaired electrons tend to have their spins in parallel. In the picture, up and down arrows symbolize the two different spin directions of the electrons (which are assigned values of +1/2 and -1/2, respectively). Unpaired electrons are highlighted in yellow. In the low spin state, four of the five electrons form two pairs of anti-parallel spin, and one orbital hosts the last, single electron. In the electron pairs, spin is canceled (+1/2 -1/2=0), and the total spin of the system is just the spin of the lonely electron (total spin=1/2). In mid and high spin the five electrons are distributed differently, such that there are three and five unpaired electrons, yielding an overall spin of 3·1/2=3/2 and 5·1/2=5/2. The integer numbers in the state symbols, ²A, ⁴A and ⁶A, refer to the so-called multiplicity M, where M=2S+1. Figure adapted from Ref.³⁶.



D) Review of previous theoretical work on CYPs

Cytochrome enzymes feature a heme-group with an Fe in the center. The oxidation of substrates involves a complex cycle, in which the central Fe-atom undergoes various changes of oxidation state as well as spin couplings (for a review, see Ref.³⁷). It is assumed that substrates (as well as inhibitors) bind to a so-called resting state (Figure 5). In the resting state, a water molecule occupies the sixth coordination site of Fe. Inhibitors, as well as substrates, expel this water molecule and take its position as the sixth coordination partner of Fe. Experimentally it is known³⁸ that the ground state of the resting state has low spin coupling, e.g. that there is only one unpaired electron.

In the resting state, the hydration of the active site and the importance of water molecules for stabilizing the electronic structure of the heme-iron were investigated via advanced calculations by Schöneboom and Thiel³⁶. For the progress of the catalytic cycle, a key step is that the enzyme goes from the resting state to the five-coordinated state, which then exhibits high spin coupling. Binding of inhibitors, e.g. triazoles, prohibits this step; as a consequence the enzyme cannot create the oxidation potential it requires for its function. The molecular mechanism for how triazoles actually do expel water and bind to the resting state was investigated by Balding et al.³⁹, again based on calculations, using a minimalistically small model system.

From these calculations we drew confidence that quantum chemistry, more precisely Density Functional Theory (DFT)³⁴, would be a good starting point for our own calculations.

E) Outline of the calculation procedure

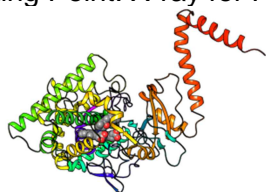
A more detailed account of how the calculations were performed will be provided by a publication which is in preparation; here, only a brief outline is presented, which may be skipped by readers not interested in computational details. Figure 6 provides a graphic overview of the procedure.

From an X-ray co-crystal structure³¹ of Yeast CYP51 in complex with PTZ-desthio^a, the active sites were extracted (Steps 1 and 2 in Figure 6). Hydrogen atoms were added because they are not observable directly in the x-ray experiment (Step 3). From the structures so far obtained, hypotheses for binding of PTZ were created by mutating PTZ-desthio's triazole moiety into PTZ' triazolelinethione, as explained in more detail later in the text (Step 4).

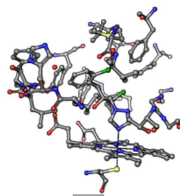
It is not really possible to calculate the full enzyme at DFT level of theory. Thus we chose the most relevant parts of the active site of the enzyme presumed to be interacting with PTZ-desthio as well as PTZ; these turned out to be 14 amino acids and two water molecules, which obviously are tightly bound by the active site and may contact the ligands; it may sound surprising that individual water molecules can play such an active role in protein-ligand interaction, but actually this is quite common⁴⁰ (see also Figure 2c).

^a All results presented here will refer to S-enantiomers, as the focus of the discussion will be on the comparison between PTZ and PTZ-desthio. The R-enantiomers can be treated by a completely analogous procedure and deliver results closely resembling the ones for the S-enantiomers.

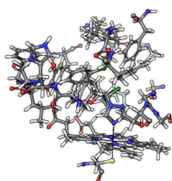
1) Starting Point: X-ray for PTZ-desthio bound to yeast CYP51 as “ template”



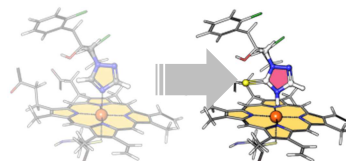
2) Extract active site



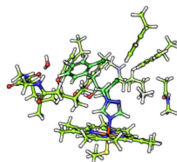
3) First modelling step: add hydrogen atoms



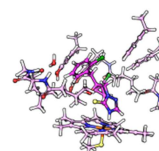
4) In-silico mutation of PTZ-desthio to PTZ to arrive at a first guess for binding of PTZ



5) Reduce to model-system capturing the interactions, but small enough for calculation



Active site model with PTZ-desthio



Active site model with PTZ

6) Quantum Chemical Geometry optimizations for all at three multiplicities

$$\hat{H}|\psi\rangle = E|\psi\rangle \quad \hat{H}|\psi\rangle = E|\psi\rangle \quad \hat{H}|\psi\rangle = E|\psi\rangle$$

$$\hat{H}|\psi\rangle = E|\psi\rangle \quad \hat{H}|\psi\rangle = E|\psi\rangle \quad \hat{H}|\psi\rangle = E|\psi\rangle$$

7) Identify best spin-state, continue with this one only

$$\hat{H}|\psi\rangle = E|\psi\rangle \quad \hat{H}|\psi\rangle \neq E|\psi\rangle \quad \hat{H}|\psi\rangle \neq E|\psi\rangle$$

$$\hat{H}|\psi\rangle = E|\psi\rangle \quad \hat{H}|\psi\rangle \neq E|\psi\rangle \quad \hat{H}|\psi\rangle \neq E|\psi\rangle$$

8) calculations and analysis from here:

- Analysis of calculated 3D geometries
- Analysis of calculated electron densities and binding mode details
- Estimation of binding affinity from calculation of enthalpies of binding

Figure 6: Schematic outline of calculation procedure (see text for details)



In the next step (Step 6 in Figure 6), the resulting coordinates were submitted to quantum chemical optimizations of the geometries, at so called DFT level of theory^{b, 41, 42, 43, 44, 45, 46, 47, 48, 49}. In this procedure, the positions of the nuclei (=atom positions in space) are optimized and an energetically optimal wave function is calculated. This was done for the three possible spin couplings of iron at the heme (see Figure 5), leading to a total of 6 geometry optimization runs for PTZ-desthio and PTZ. In order to mimic the steric influence of the entire protein, in each amino acid residue the position of one atom was fixed (we chose a carbon as close to the protein backbone as possible). All other atoms, including the entire ligands and the water molecules, were allowed to move freely. All in all, the models comprise ~300 atoms with about ~1000 electrons.

In Step 7, the energies of the different spin states were compared, and in the following, only the results for the energetically most favorable spin state will be further discussed. This step may appear a little overdone, as we know the optimal spin state from experiment; however, it will be important here to validate our choice of level of theory as well as our choice of model system.

The calculations from Step 6 deliver:

- 3D geometries, or more precisely: 3D coordinates for each atom in the model systems. These geometries provide first clues about how the ligands bind to the active site. (Step 8a)
- Wave functions, from which electron densities can be calculated. Analysis provides details of the mode of binding and the relative importance of different interactions between the ligand and the active site. (Step 8b)

For Step 8c, an estimation of the relative binding affinity of the different ligands, additional calculations on the free ligands were required, which followed a very similar DFT-protocol as the optimizations in Step 6.

Anticipating the discussion below, it is worth emphasizing that the geometry optimization delivers **only** 3D coordinates of nuclei, not directly bonds. Most of the respective figures will show bonds, which are just graphical connections of the atom positions, based on chemical experience and a set of rules. The inner nature of the bonds can be determined by analysis of the wave function and the electron density, as set forth in later paragraphs. However, in almost all cases, also the “bonds” we draw by chemical intuition are indeed bonds that are confirmed by analyzing the electron densities.

It should be noted that as of today, no other calculations involving analysis of electron density topology have been published on comparable systems⁵⁰.

^b A little more precisely, we employed the Becke and Perdew BP86 combination of functionals^{41,42}, along with Ahlrichs' def2-TZVP basis sets⁴³. Grimme's D3 dispersion correction⁴⁴ was employed to overcome DFT's notorious weakness in describing non bonded interactions. Relativistic effects due to the core of the heavy metal iron were taken into account by the ZORA⁴⁵ approximation. We used the program packages ORCA^{46,47} for performing the quantum chemical calculations and AIMStudio⁴⁸ for subsequent QTAIM-analysis. Molecular modelling was done with Maestro⁴⁹.



F) Validation of the computational procedure by comparing calculation results with experimental data available for PTZ-desthio binding to CYP51

Before creating and interpreting a hypothesis for the mode of binding of PTZ, it is important to check the validity of the calculation procedure. This is done by comparing the calculation results for PTZ-desthio with the available experiments.

Checkpoint 1: Is the spin coupling at Iron described correctly?

As stated above it is known³⁸ from spectroscopic studies that triazole inhibitors bind typically to a low-spin state of the iron of CYPs. Our calculation clearly confirm this, as the low spin state is by far the energetically most favourable situation, see Figure 7.

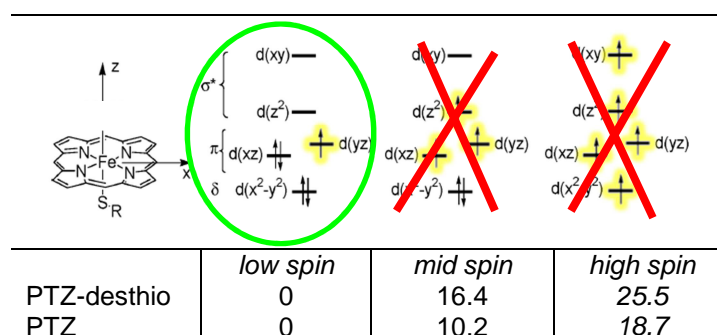


Figure 7: Relative total energies in kcal/mol of the model systems at Density Functional level of theory

⇒ So, as a first quality check, it can be stated that the calculations describe spin coupling in the CYPs in alignment with experiment.

Checkpoint 2: Are the calculated geometries for binding of PTZ-desthio close to the X-ray data?

Next, the geometries of the models optimized at DFT level of theory were compared with the respective X-ray-geometry (Figure 8). By construction, the positions of 14 C-atoms were fixed, thus their perfect alignment with the X-ray-geometries is not surprising. However, as the figure clearly shows, there is not much movement of the remaining more than 260 atoms, neither in the side-chains, nor in the PTZ-desthio ligand due to the optimization. Notably, this is also true for the position of the water molecules in the pocket.

Highlighting another feature, which will be discussed in more depth below, the calculated distance between N-4 of the triazole head-group of PTZ-desthio and the heme iron is 2.1 Å. Considering the resolution of the X-ray structure of ~2 Å, this compares very well with the distance from the X-ray coordinates, which is 2.2 Å.

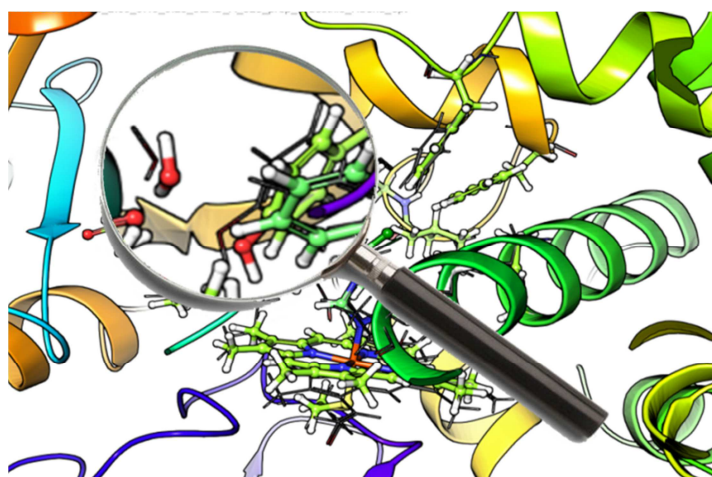


Figure 8: PTZ-desthio binding to yeast CYP51: Comparison of optimized model structure with experimental crystal structure

Overlay of calculated structure (ball and sticks) and X-ray data³¹ (ribbons and wireframe atoms, from PDB-ID 5EAD). For clarity, hydrogen atoms were added to the X-ray data as well. The magnifying glass highlights one water molecule and a neighboring tyrosine-residue. Note how close the experimental and calculated positions are to each other.

⇒ **From this we may conclude that both the level of theory as well as the choice of residues, adequately describe the experiments. Thus, we may confidently interpret the calculations on PTZ as well.**

G) Binding modes of PTZ and PTZ-desthio are fundamentally different, with respect to Geometry, Topology as well as Binding Strength

With the confidence gained from the calculation on PTZ-desthio, we may interpret analogous models created for PTZ. No X-ray template was available for the creation of the PTZ models. As already briefly stated, we used the X-ray co-crystal structure for PTZ-desthio, but “mutated” the triazole-head of PTZ-desthio into a triazolinethione, thus arriving at a model for PTZ. By this procedure, the hydrogen of the NH-moiety of the triazolinethione came very close to the heme-iron, which obviously cannot be a reasonable starting point for optimization (See Steps 4 and 5 in Figure 6).

From theoretical pre-studies we knew that methyl-triazolinethione preferentially binds to heme with the sulphur-atom of the triazolinethione complexing the heme-iron^{c,51}. Thus we manually adjusted the dihedral angles in the “mutated” geometries to arrive at energetically less stressed conformations. The active site residues were not touched. With the starting geometries generated in this way, geometry optimizations were performed following the same protocol as outlined for PTZ-desthio.

^c Results not shown here. In a nutshell, we tested binding of just methyl-triazole and methyl-triazolinethione to a heme, with methyl-thiolate as the sixth coordination partner for iron. The basic idea is similar to Ref.⁵¹. Several different starting geometries were chosen, such that all N-atoms as well as triazolinethione’s S-atom were oriented towards the heme iron. Clearly, triazoles prefer binding via the nitrogen atom at position 4 over binding via the other two Ns, which exactly reflects the situation found in classical triazole “type II” binding to CYP-Enzymes. In methyl-triazolinethione, complexation of iron via the S-atom is the energetically most favorable option.

i) The 3D binding-pose of the PTZ-headgroup to heme differs significantly from that of triazoles, while PTZ-desthio's triazole moiety shows the triazole-typical binding pose.

Finding #1: The binding mode of PTZ is different from that of PTZ-desthio

Figure 9 shows the final geometries of the models for binding of PTZ-desthio and PTZ to our CYP51 model. PTZ-desthio's triazole head binds centro-symmetrically with respect to the heme group, just as expected for triazole typical type II binding. In PTZ, however, by binding via the sulphur atom, the triazolinethione head is significantly shifted off-center of the heme.

This is a first argument explaining why binding of PTZ is of a different type compared to triazoles (compare Figure 1).

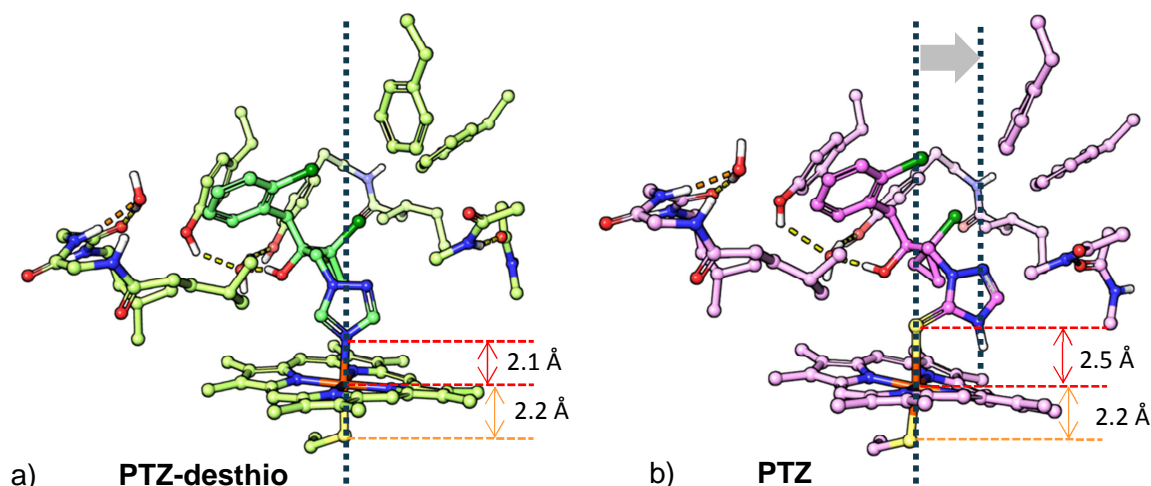


Figure 9: Comparison of binding modes of PTZ-desthio and PTZ, part 1: Geometric differences

While the triazole head of PTZ-desthio binds centro-symmetrically with respect to the heme, PTZ's triazolinethione is shifted off-center and binds to the heme-iron via Sulphur (see vertical, black dotted lines). Red and orange dashed lines indicate the distances between the heme iron and its two axial binding partners, the thiolate "below" the heme moiety, and the PTZ-desthio and PTZ head group. See text for discussion.

Interestingly, the off-center shift of the triazolinethione head group is possible without the need to significantly displace the positions of the amino acid residues. This fits to the earlier mentioned observation that the orientations of the active site residues in the X-ray co-crystal structures of different azoles remain surprisingly close to each other³¹.

Finding #2: Bond lengths provide first hint of weak binding of PTZ

As already stated, in the PTZ-desthio-CYP51 complex the distance between the heme iron and N-4 in the triazole head is 2.1 Å. This value is very close to N-Fe distances in comparable molecules for which high precision small molecule X-ray data are available^d. PTZ-desthio thus seems to bind very tightly to the heme.

^d On 2018 March 19th, a search in the Cambridge Crystallographic Database (CCDC) gave Fe-N distances of 1.990 Å, 2.003 Å and 1.937 Å in systems in which Fe was hosted by a heme-like system and N and S were axial ligands (CSD codes: KULWOD, PIMVFE01, and SAXTEQ)



In the case of PTZ, however, the triazolinethione-S-Fe distance is longer than expected for an ideal Fe-S bond: From comparison to similar small molecular systems^e, one would expect Fe-S bond lengths of ~ 2.2 to 2.3 Å, not 2.5 Å as in our PTZ-model.

For comparison, the bond lengths of the other Fe-S bond, the one to the thiolate (“below” the heme in Figure 9) are 2.2 Å when binding either PTZ or PTZ-desthio. While this second Fe-S bond is really tight, the relatively long triazolinethione to heme bond provides first evidence that PTZ binds weaker to CYP51 than PTZ-desthio.

3rd Intermezzo: Quantum Theory of Atoms in Molecules (QTAIM) provides a rigorous, yet intuitive approach to chemical structure and the chemical bond.

This paragraph may be skipped by readers experienced in computational chemistry.

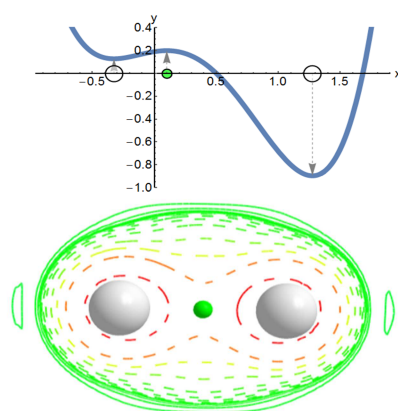


Figure 10: Classroom mathematics are the basis for QTAIM

Top: Recall from calculus classes: a simple function $f(x)$ as a blue line. Location of two minima shown as white dots and one maximum in green.

Below: Contour diagram of the Laplacian electron density for the H_2 molecule. The white spheres (“Nuclear Critical points”) indicate the positions of the two nuclei. The green sphere shows a bond critical point, which is just at the center of the chemical bond.

According to an often quoted anecdote⁵², the spectroscopist E. Bright Wilson, at an early conference on Density Functional Theory in 1965, suddenly stood up and spontaneously proclaimed that he now had understood the theory: If one only knew the electron density ρ of a molecule and nothing else, the cusps of ρ would tell where the nuclei are, the gradient at these points would tell the nuclear charge, hence the element, and finally the integral over all space would yield the number of electrons. In summary, all properties of the molecule are somehow encoded in the electron density. 1994, R.W. Bader published a book “Atoms in Molecules: A Quantum Theory”, in which he outlined the basics of QTAIM. In a nutshell, it translates E. Bright Wilson’s observation to algebra and calculus.

You may remember differential calculus from school, taking the derivative of functions to identify extremal points and turns in graphs, like in the example shown left. The electron density is just a function in three-dimensional space, but derivatives and second derivatives are computed using the same mathematics, leading to the location of saddle points. As the electron density is a function of three dimensions, x,y,z , there are four different types of saddle points. Only two are of interest for us here, “nuclear critical points” (NCPs) and “bond critical points” (BCPs). NCPs coincide with the position of the atomic nuclei. BCPs show the charge center of a chemical

bond. Critical points can be connected by critical paths, which can also be rigorously computed. Bond critical paths connect nuclei (NCPs) and pass through bond critical points (BCPs). **Bond critical paths are nothing else but physics-based representations of chemical bonds.** The results of a QTAIM analysis can be visualized as a QTAIM graphs in 3D, see Figure 12. If such a graph shows only the NCPs and the bond critical paths, the QTAIM graph looks surprisingly

^e Another search on 2018 March 19th in CCDC for heme-like systems with two axial S atoms complexing Fe gave the following Fe-S distances (In Å, CSD-Code in parenthesis): 2.337 (BAVPOD), 2.310 (DIDCEY), 2.336 (KCROFE), 2.222 (RIRBAW), 2.307 (SPCNFE), and 2.339 (TPHF10)



similar to ordinary molecular modelling pictures, with the decisive difference that the bonds are not drawn by some (in essence arbitrary) set of rules, but based on the topology of the electron density. The graph is chemically intuitive, but at the same time unbiased by any prejudice on how the bonds should look like. QTAIM thus provides a nice way to investigate molecular systems and the bonds in and between them.

ii) Analysis of the electron densities shows that also the electronic modes of binding of PTZ and PTZ-desthio differ significantly

Analysis of binding modes in purely geometric terms, i.e. distances and angles, is straightforward and temptingly easy; it is safe to assume that the interaction between two atoms becomes weaker, the larger the distance between the two becomes. The converse statement, however, is not necessarily true. When the distance between two atoms becomes short, this does not necessarily mean that the two atoms actually form a chemical bond. It may well be that their spatial proximity is driven by packing effects, which means that the observed proximity of the two atoms is not driven by this pair of atoms itself, but by other inter- (or intra-) molecular forces involving other atoms. Protein-ligand complexes are typically “crowded” systems, with many interacting moieties, as shown in the inlay. Purely from the inter-atomic distances it is thus not possible to distinguish between situations, in which proximity of two molecular entities is driven by mutual attractive forces, or rather by interactions between other molecular entities^f.

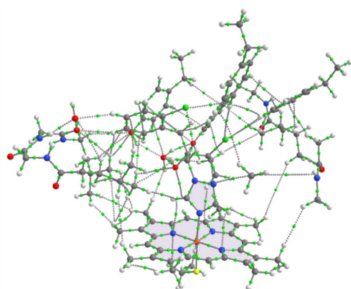


Figure 11: Illustration of the crowdedness of the active site

All interactions between the more than 270 atoms of the PTZ-desthio/CYP51 model, as derived from the calculated electron density by QTAIM analysis. Note, how crowded and how densely packed the system really is.

Fortunately, chemical interactions are completely contained in the topology and structure of the respective electron densities. Unfortunately, the resolution of experimental electron densities, especially for large systems like proteins, is not sufficient for topological analysis. The results from the quantum chemical calculations, however, can be analyzed in the frame of the quantum Theory of Atoms in Molecules (QTAIM)⁵³. QTAIM has already been successfully used to study bio-molecular systems, recently also in the context of ligand protein interactions^{50,54}.

The electron densities arising from our calculations were subjected to QTAIM analysis. Some details from the resulting QTAIM graphs are shown in Figure 12.

The small green spheres in the graphs show the bond critical points (BCPs). A charge density is associated to each BCP. The stronger a bond is, the higher is the charge at a given BCP. Bonds shown as broken lines in the figure have BCPs with charges below 0.05 atomic units (“weak interactions”), bonds with higher BSP charges are shown as full tubular lines.

^f Using a little far-fetched analogy, on a crowded dance-floor in a discotheque or at a rock concert you will find a lot of closely proximal dancers, where the proximity just results from packing, not from mutual attraction. But conversely, groups of friends or lovers will be found close to each other with high probability.

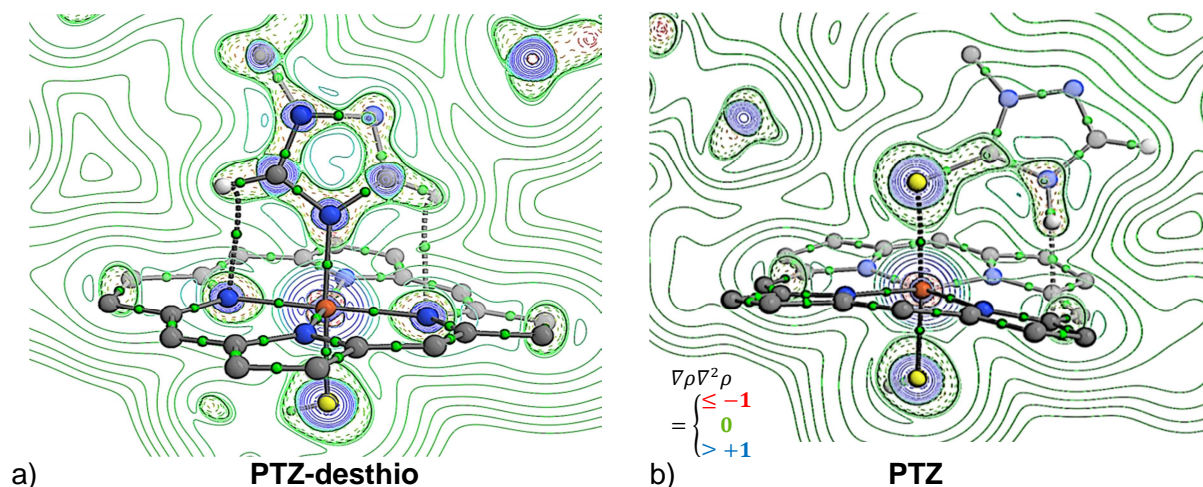


Figure 12: Comparison of binding modes of PTZ-desthio and PTZ, part 2: Electronic differences

Both panels show excerpts of the full QTAIM graphs (compare Figure 11), highlighting just the interaction of the triazolinethione group of PTZ-desthio and the triazole group of PTZ with the heme function. The graphs result from an analysis of the respective electron densities of the full model systems. Large spheres indicate calculated positions of atomic nuclei, with colors indicating the elements (C: gray, H: white, N: blue, Fe: orange and S: yellow). Small green spheres indicate positions of bond critical points. Tubular lines show the calculated chemical bond paths, with bond critical charges > 0.05 a.u. Weak bond paths, with charges lower than 0.05 a.u. are shown as broken tubular lines. The contour diagram shows the Laplacian of the electron density in a plane that intersects some key atoms. See text for details.

For comparison, H-bridges involving one of the two water molecules in the models are shown as broken lines, the respective charges range between 0.02 to 0.03 atomic units (a.u.). We will use a value of 0.02 as a reference value for comparisons, referring to it as the “water-hydrogen-bond”-charge.

Finding #3: The electronic topologies of binding to the heme group are fundamentally different for PTZ and PTZ-desthio, with the PTZ-desthio headgroup binding tighter to the heme

As stated in section 5 B), PTZ-desthio binds (like triazoles) in a “type II”-mode, while PTZ gives rise to weaker, triazole-atypical binding. It was already assumed in the cited experimental studies that these differences may be caused by differences in the electronic details, how the molecules bind to the heme-Fe. Atomistic details underpinning this assumption, were, however, missing.

Figure 12 provides electronic reasoning for this assumption. PTZ-desthio binds to the center of the heme only, with a major bond to the central iron atom, plus one or two secondary interactions with the heme nitrogen atoms. The BCP connecting the N-4 atom with iron features a charge of ~ 0.08 atomic units, which is approximately four times our “water-hydrogen-bond”- reference value of 0.02. For this reason, the respective bond path is shown as a regular bond with a solid line in Figure 12a). The two secondary interactions connect the two hydrogen atoms of the triazole head to heme-N-atoms. These are much weaker ($\sim 1/2$ the charge of a “water-hydrogen-bond”). In contrast, the triazolidinethione of PTZ shows two weak interactions to heme. The stronger one of these, connecting the triazolidinethione S with Fe, features a BSP

charge that only doubles our “water-hydrogen-bond”-reference value, thus staying below the threshold of a weak bond, and is shown as a dashed line in panel b). As a very weak secondary interaction, one H-atom of the triazolidinethione-head interacts with a pyrrolic carbon atom in the heme ring.

In conclusion, electronic topology of heme binding modes of PTZ-desthio and PTZ reveals *qualitative differences* (in terms of bond charges) as well as *quantitative differences* (in terms of interaction partners in the heme group). The PTZ-desthio head group is clearly the better binding partner for heme.

Finding #4: Molecular features common to both PTZ and PTZ-desthio lead to similar interactions, contributing to, and modulating, overall affinity

With the exception of the triazole/triazolinethione head-groups, PTZ-desthio and PTZ are identical. It is thus not surprising to find that the identical parts of the two ligands feature similar interactions with the active site. Indeed, the 2nd-strongest interaction after the head-group heme interaction for both PTZ-desthio and PTZ, is a hydrogen bridge connecting the hydroxyl functions of PTZ-desthio and PTZ to the conserved water-molecule W743 (Figure 13).

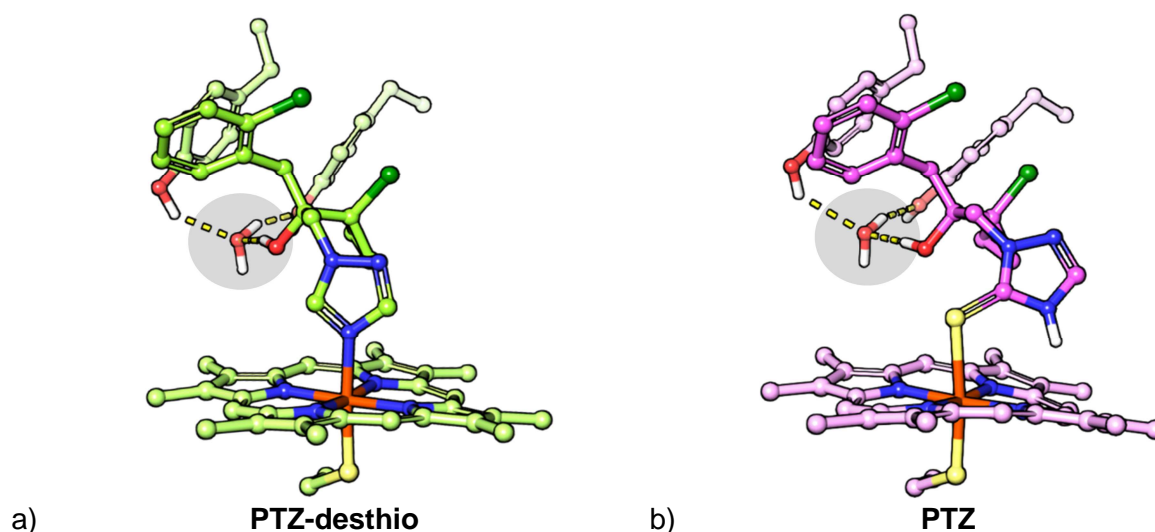


Figure 13: Comparison of binding modes of PTZ-desthio and PTZ, part 3: Common features

The “side chains” of PTZ-desthio and PTZ are identical, and also show similar interactions with the active site. The figure shows one such common feature, a strong hydrogen bond to a water molecule, which mediates binding to tyrosine-residues of the active site. See text for details.

W743 in turn interacts with the hydroxyl functions of tyrosine residues Y126 and Y140 and is thus tightly bound, explaining why this water molecule is experimentally observable in X-ray studies. In yeast mutants, in which Y140 is replaced by phenylalanine or histidine (Y140F or Y140H), the affinity of PTZ and PTZ-desthio is significantly reduced³¹. Part of this may be attributed to W743 losing one binding partner, weakening its integration within the binding site and thus indirectly loosening binding of the ligands as well. Our model thus even provides atomistic understanding of how these mutations affect binding.

iii) In terms of binding enthalpy, PTZ-desthio binds significantly more strongly to CYP51 than PTZ

After investigating the mode and electronic topology of binding of PTZ and PTZ-desthio enantiomers, we wanted to provide semi-quantitative estimates of their relative binding affinities. Figure 14 illustrates the task as well as its challenges.

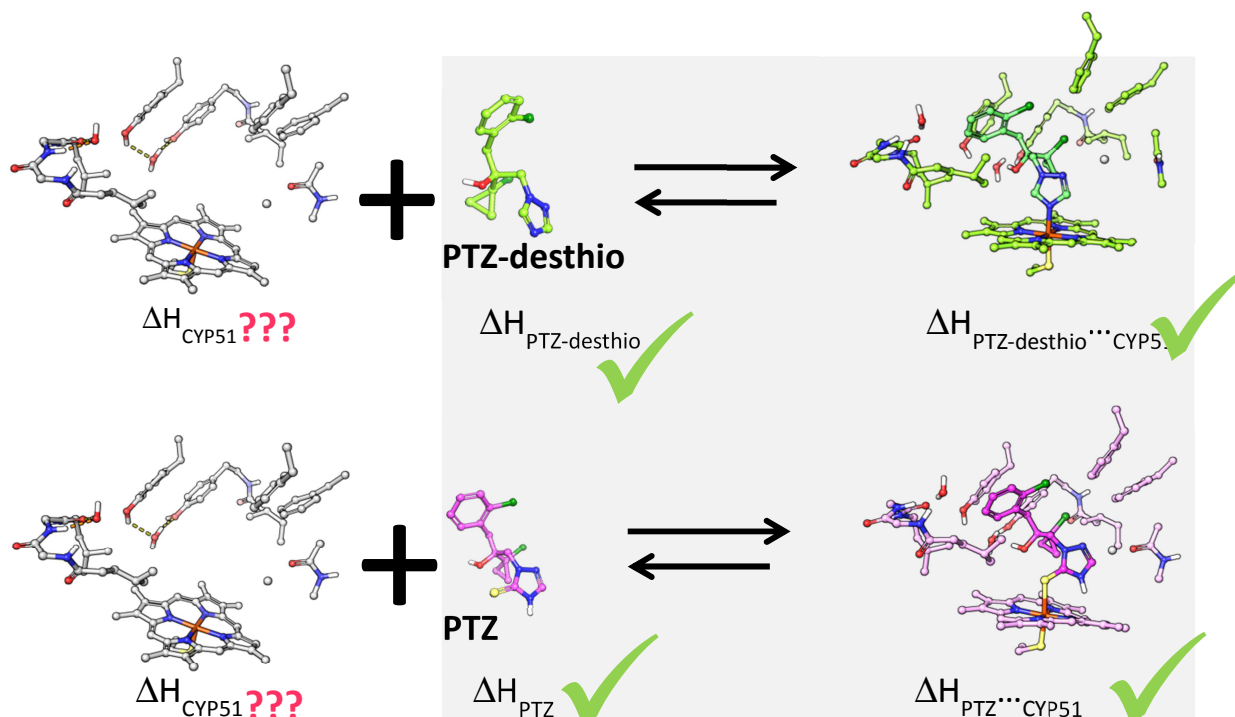


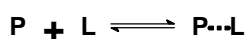
Figure 14: Illustration of how the energetic difference between binding of PTZ-desthio and PTZ to CYP51 was estimated

The green slashes indicate energy-values (“ ΔH ”), which are readily available from our calculations. The energy ΔH_{CYP51} , of ligand free CYP51, is not as easily computed, and hence marked with red question-marks. See text for details.

4th Intermezzo: Chemical equilibria, binding affinity and binding energies

This Intermezzo may safely be skipped by readers familiar with chemical thermodynamics

The K_d values obtained experimentally from a biochemical test describe a dynamic equilibrium as shown in Figure 14. Imagine, in the beginning of your experiment that you have only free protein in solution. Then you add free ligand to the solution. The ligands then may bind to the protein, forming a protein-ligand complex. However, these complexes do not last indefinitely. Instead, the ligands will dissociate from the proteins, forming again free ligand and free protein, will bind again and again dissociate. This is a highly dynamic process. After some time, the process will “equilibrate”, such that **macroscopically** the concentrations of free ligand, free protein and protein-ligand complexes will remain constant. At the molecular level, also at equilibrium, protein-ligand complexes continue to dissociate and re-associate back and forth. In the language of chemistry:





In high affinity ligands, this dynamic equilibrium will lie more to the “right” side of the arrow, on the side of ligand-protein complexes, whereas for weak binding the balance will favor the “left” side with free ligand and protein.

It can be shown by basic thermodynamics that the K_d -value quantifying this equilibrium is related to the free energy difference ΔG_{equi} of the left and the right side via $\Delta G_{\text{equi}} = -RT \ln K_d$. (where R is the gas constant and T is the absolute temperature). The free energy ΔG_{equi} can easily be computed from the individual free energies via $\Delta G_{\text{equi}} = \Delta G_{P\dots L} - \Delta G_P - \Delta G_L$.

*Here is where trouble starts. First, our calculations do not deliver **free energies** ΔG , but **enthalpies** ΔH . If we would know the so-called entropies ΔS , which measure the degree of order in a system, we could calculate the free energies via $\Delta G = \Delta H - T \cdot \Delta S$. However, entropies are not directly available in our approach. Fortunately, we can safely assume that the involved entropies in free PTZ-desthio versus free PTZ, and CYP51...PTZ-desthio versus CYP51...PTZ are comparable. Thus they will cancel out in the differences.*

*As indicated by green slashes in Figure 14, the enthalpies for the free ligands and the protein ligand complexes are readily available from our calculations. This leads us to the second issue: It is not easy to define a reasonable reference state for the free protein. As set forth above, the resting state is not an empty protein leaving the sixth coordination of Fe unsatisfied, but rather filled with water. Fortunately, the protein is the same irrespective of whether PTZ-desthio or PTZ is binding. Thus, if we only restrict discussion to the **difference** in the binding affinity of **PTZ-desthio versus PTZ**, the energy of the free protein cancels out.*

Finding #5: PTZ' affinity to CYP51 is weaker than that of PTZ-desthio by several orders of magnitude

The difference in the binding enthalpies of PTZ-desthio binding to CYP51 versus binding of PTZ to CYP51 is:

$$\Delta H_{\text{PTZ-desthio vs. PTZ}} = \Delta H_{\text{PTZ-desthio}\dots\text{CYP51}} - \Delta H_{\text{PTZ-desthio}} - (\Delta H_{\text{PTZ}\dots\text{CYP51}} - \Delta H_{\text{PTZ}}) \approx -11 \text{ kcal/mol},$$

this is a large difference. Under the assumption that entropic contributions cancel out in this difference, this readily explains why PTZ binds several orders of magnitude less strongly to CYP51. As a rule of thumb, a difference of 1.4 kcal/mol in free energy corresponds to a factor of 10 in terms of affinity. This value is clearly in line with the biochemical and spectroscopic results in Table 1, and provides atomistic reasoning as to why the binding of PTZ is so much weaker than that of PTZ-desthio.

In order to further validate these energy differences, single-point calculations are under way at the highest available correlated ab-initio method available, so-called linear scaling coupled cluster theory (“DLPNO-CCSD(T)”⁵⁵). This level of theory is known to deliver “chemical accuracy”, i.e. energies with errors below 1 kcal, but is also notorious for its hunger for computer resources, which, before the advent of linear scaling variants, prohibited any application for systems as large as the one under study here. Preliminary results confirm the findings of the DFT results shown here.

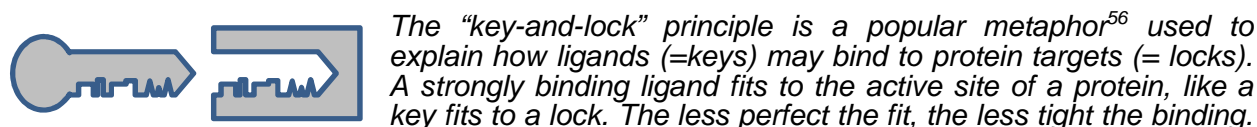
H) Summary of the quantum chemical calculations

- The overall energetic/enthalpic driving force for binding PTZ-desthio is significantly higher than for the PTZ molecule, rendering PTZ's affinity to CYP51 very low.
- The modes of binding of PTZ and PTZ-desthio differ fundamentally, especially when considering how the head groups bind to the heme of CYP51.
- The differences between PTZ and PTZ-desthio can indeed be attributed to their different head groups, while the rest of the ligands show comparable interactions.

Together, these atomistic findings explain the decreased affinity of PTZ to the target CYP51 compared to PTZ-desthio. Figure 15 provides a graphical version of this summary, employing a “key-and-lock” metaphor.

5th Intermezzo: The simplistic “key-and-lock” picture.

This paragraph may be skipped by readers experienced in bio-physical chemistry.



Although this metaphor is easy and grippingly intuitive, the picture has fundamental flaws:

- The picture is static. In reality, ligands do not bind to a protein and stay there indefinitely, but there is a dynamic equilibrium of ligands entering, binding and leaving the active site of a protein (this dynamic equilibrium is quantified by the K_d values, compare 4th Intermezzo).
- The key and the lock are rigid. In reality, both ligand and protein are flexible. They can and also do frequently adjust their shapes to mutually accommodate and even increase binding strength.

However, if used with care, the picture is still instructive.

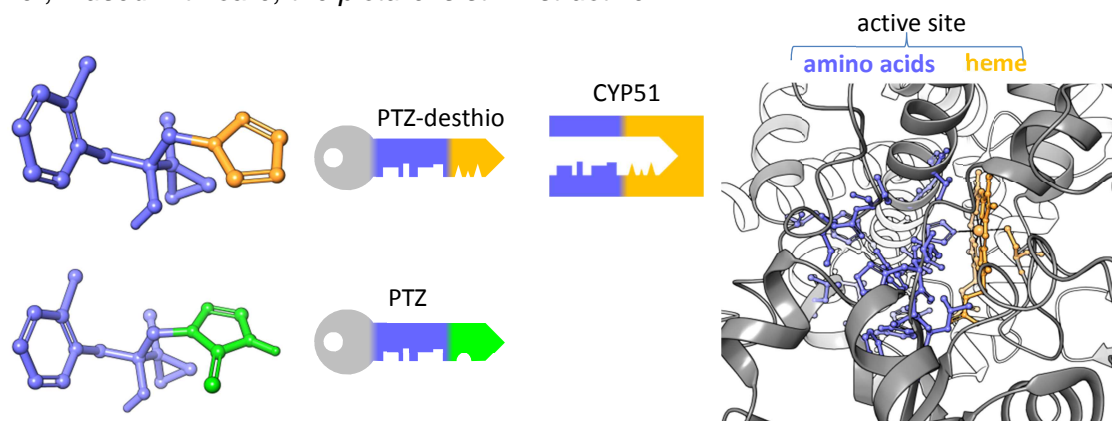


Figure 15: Simplistic „key-and-lock” analogy for the binding of PTZ and PTZ-desthio to CYP51

As shown by the quantum chemical calculations, differences of binding of PTZ and PTZ-desthio to CYP51 can be very much reduced to differences of binding due to the different head groups. The right hand side shows the active site of CYP51 (caution, the picture is tilted by 90° counter clockwise compared to all previous figures showing the active site). Atoms of the heme group are shown in orange, the amino acids of the active site are shown in blue. The structures of PTZ-desthio and PTZ are shown on the left. Their common features are shown in blue. The triazole head is shown in orange, the triazolinethione head in green. The two keys and the lock in the center translate the molecules to our “key-and-lock” metaphor. The orange triazolinethione-tip of the PTZ-desthio key matches perfectly the orange heme-part of the lock, while the green tip of PTZ matches far less nicely to the heme. The blue parts of both keys match the blue amino acid part of the lock very well. However, it is the green tip of PTZ that prohibits good binding of PTZ to CYP51.



I) Based on the CYP51 findings, conclusion by analogy allows similar trends to be expected for CYP19 and CYP26

From the quantum theoretical calculations, in concert with the experimental evidence, we have shown that the triazolinethione head of PTZ gives rise to weak and triazole-atypical binding to yeast CYP51 in contrast to the strong type II binding of many known inhibitors with triazole-like heads, including PTZ-desthio.

It would be desirable to perform analogous calculations to arrive at binding mode hypotheses for PTZ and PTZ-desthio to CYP19 and CYP26, as these two are known to be key players for understanding toxic effects in the class of classical triazole fungicides.

Unfortunately, such calculations cannot be performed without compromising the predictive rigor of the approach.

For CYP26, three distinct enzymes (CYP26A1, -B1 and -C1) are found in *H. sapiens*⁵⁷, and for none of these is an X-ray structure available⁹. Homology models for human CYP26s have been created internally, based on the closest homolog for which an X-ray structure is available⁵⁸; CYP120A1 from *Synechocystis sp. PCC 6803*. It also binds to the retinoic acid as CYP26 does. The average sequence identity between this template and the human CYP26s is about 34%. Further CYP26 homology models were created by Buttrick⁵⁹, combined with docking calculations. While these models are instructive, their precision is not a sufficient basis for quantum chemical calculations.

The situation is better for CYP19A1, for which at least 11 crystal structures are available⁹. However, these structures are either ligand-free or are in complex with sterol-like ligands.

Thus, for CYP26 and CYP19, we do not have a high quality X-ray structure with which to start quantum chemical calculations. Any such calculation would become too speculative.

We therefore decided to address this point via a conclusion by analogy approach. For this purpose, we compared the overall shapes of the active sites of various CYPs (Figure 17).

Finding #6: CYP51, CYP19 and CYP26 all feature a heme and their overall architectures are comparable

Figure 16 shows that the overall shape in terms of loops and helices of yeast CYP51, human CYP19, and human CYP26 are indeed very similar. The overlays were created by alignment for the Heme-moieties only. If the overall protein would have been used for alignment, the similarity of the loops and helices would be even more striking. Here, however, we wanted to focus attention on the heme in the active sites.

⁹ PDB query was performed 19-01-2018.

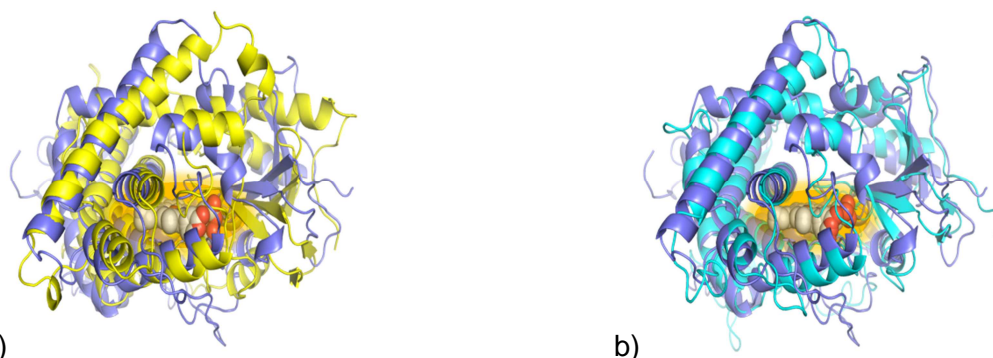


Figure 16: Common architecture of yeast CYP51 (in blue), human CYP19 (yellow) and human CYP26 (cyan)

Panel a) shows an alignment of CYP51 with CYP19, panel b) compares CYP51 with CYP26. Alignments were created by overlay of just the common heme group, which is highlighted by an orange glow. 3D structures were taken from the protein data banks³²: *S. cerevisiae* CYP51 (Blue, PDB ID: 5EAD); *H. sapiens* CYP19 (Yellow, PDB ID: 3S79), *H. sapiens* CYP26A (Cyan, homology model). See text for details.

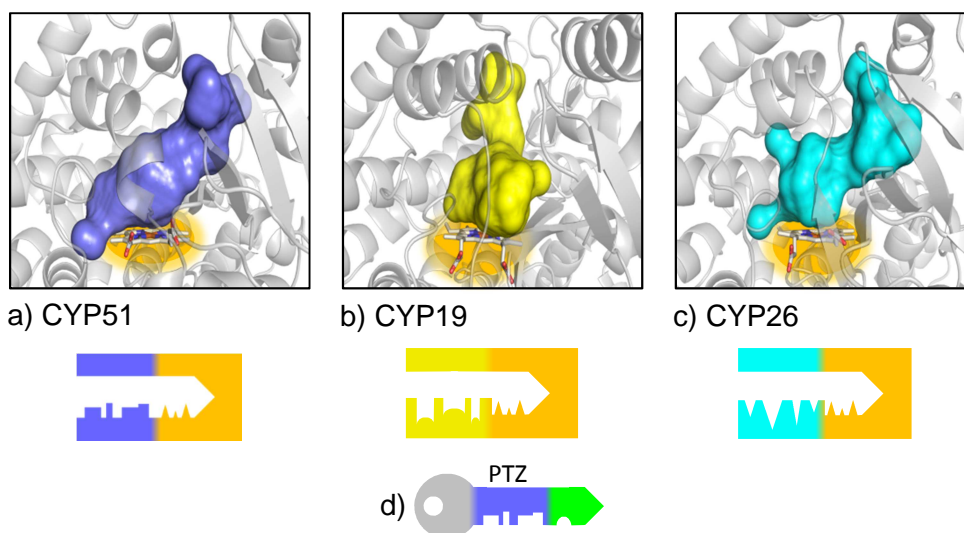


Figure 17: Differences among active sites and active site channels in a) yeast CYP51, b) human CYP19 and c) human CYP26

Color coding and PDB-IDs as in Figure 16. Again, the common heme function is highlighted by an orange glow. Below panels a) to c) you find cartoon “locks” for our “key-and-lock” metaphors, analogous to Figure 15. Panel d) recalls the key-methaphor for PTZ from Figure 15.

Finding #7: The shapes of the active sites of CYP51, CYP19 and CYP26 reveal differences, although the overall architectures are so similar

In Figure 17, panels a) to c) zoom into the individual CYP structures; the perspective is identical in all three panels. The heme-moiety is shown as a stick model and highlighted by an orange glow; above the heme, the surfaces show the shapes of the active sites, including at least part of the entry channels. It is obvious that the high degree of similarity between the CYPs at the level of overall shape and of course the presence of a heme in all three proteins does *not* translate to high similarity of the active site shapes.



Finding #8: PTZ is unlikely to bind to any CYP, unlike triazole-like inhibitors

Translating this again into the “key-and-lock” metaphor, please refer to the locks below panels a) to c) of Figure 17. The overall architecture of the locks/CYPs is comparable; hence all locks have the same lengths. In addition, all feature an orange heme-tip. However, the details are different, symbolized by the blue, yellow and cyan parts of the locks.

The key representing PTZ features a green triazolinethione-tip which does not match any of the CYPs’ heme functionality, as has been shown by the quantum chemical studies above.

This easy metaphor also explains, why not all triazoles show identical tox profiles. In our picture, all triazoles have an orange tip, closely matching the heme. The rest of the molecule, however, allows in principle the design and modulation of the CYP profile of a compound.

J) Theoretical conclusions match experimental evidence

From this, and in conjunction with the more detailed analysis of PTZ and PTZ-desthio binding to yeast CYP51, **we may conclude that:**

- i. The triazolinethione head of PTZ will only give rise to weak and atypical binding to any CYP, as this binding feature depends in the first place only on the triazolinethione itself and the heme. This means that the triazolinethione will only marginally contribute to the binding affinity.**
- ii. Conversely, the triazole head of PTZ-desthio and triazole fungicides will quite probably show a strong tendency to bind to several CYPs.**
- iii. However, a triazole-like head group does not bind alone, but the full molecule is important. This means that the high affinity of a triazole-like compound to one particular CYP does not imply that it also shows high affinity to all others.**

These arguments are also backed by experimental evidence. As already mentioned, Kjeldsen et al. have shown that PTZ does not inhibit aromatase (CYP19)²², supporting conclusion (i.) on the weak binding of PTZ itself.

Conclusions (i.), (ii.), and (iii.) are also reflected in the publication of Warrilow et al.²⁴ showing a 149- and 23-fold lower binding affinity to fungal and human CYP51 for PTZ than for PTZ-desthio. There were also up to 7-fold differences in binding activity to fungal CYP51 among the classical triazoles with the shared feature of a triazole-head. This supports the hypothesis that differences in affinity are also dependent on the triazole side chain interaction with the CYP51 polypeptide chain. This is further supported by the results of *in vivo* developmental toxicity studies, summarized by Dimopoulou²⁶ (Table 2).



Table 2: Categorization of *in vivo* developmental toxicity potency of PTZ and different azole-type fungicides

Data from Ref.²⁶. BMD₁₀ = calculated benchmark dose resulting in 10% additional incidence of developmental toxicity.

Compound	Head group	<i>In vivo</i> BMD₁₀ (μmol/kg bw)	Potency group for <i>in vivo</i> developmental toxicity
PTZ	triazolinethione	917.8	weak
Difenoconazole (DFZ)	triazole	596.5	weak
Ketoconazole (KTZ)	imidazole	20.1	potent
Flusilazol (FLU)	triazole	9.1	potent
Micoconazole (MCZ)	imidazole	258.3	moderate
Triadimefon (TDF)	triazole	91.5	moderate
Propiconazole (PRO)	triazole	386.7	weak

With the exception of PTZ, which showed the lowest *in vivo* developmental toxicity potency, all of the other compounds featured a triazole/imidazol head, and thus bear the potential of tight binding to heme. However, by modulation due to differences in the chemical structures of the rest of each molecule, the potential for tight binding does not necessarily translate into the same developmental toxicity potency.

5) The unique metabolic detoxification principle of PTZ in humans and mammals

The already previously available Bayer AG proprietary animal and human metabolism data complete the reasoning why PTZ does not cause the reproductive toxicity associated with classical triazoles and why PTZ has a generally very low toxicity in mammals.

Following absorption in rats, PTZ was rapidly conjugated with glucuronic acid in the liver to the metabolite PTZ-S-glucuronide and excreted with the bile. The conjugation with glucuronic acid at the sulfur atom was the main metabolic reaction. PTZ-S-glucuronide was the main metabolite and was found at approx. 46% of the administered dose in the bile of rats. A comparative *in vitro* study showed that the same main metabolite occurred in incubations with human hepatocytes. The same main metabolic reaction was also found in goat metabolism studies. Thus, the S-glucuronidation of PTZ was demonstrated as the main metabolic reaction and a key detoxification route in humans and mammals. Based on the computational chemistry studies presented in the previous section, it can be assumed that also in its S-glucuronidated form PTZ cannot bind to CYP enzymes and thus cannot exhibit triazole-typical toxicological properties.

Unlike many other 1,2,4-triazole active substances, PTZ uniquely contains a 1,2,4-triazolinethione moiety. The sulfur atom protruding from the 1,2,4-triazoline moiety of PTZ is an anchor readily available for conjugation. Thus, PTZ is converted to the S-glucuronide, the polarity is increased and the excretion is facilitated (see Figure 18). The conversion to the S-glucuronide is the dominating systemic metabolism reaction and the excretion of this conjugate is rapid.

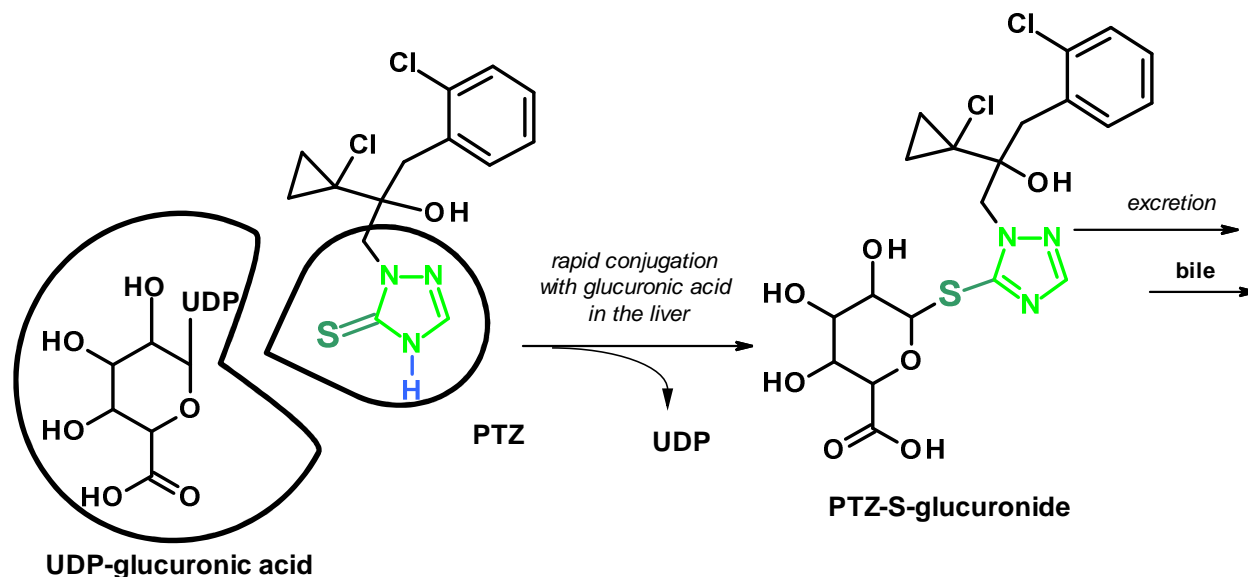


Figure 18: Detoxification mechanism of PTZ in humans and mammals

PTZ uniquely contains a 1,2,4-triazolinethione moiety and is thus converted to the S-glucuronide. This conjugation is the dominating systemic metabolism reaction and the excretion of this conjugate is rapid.



Furthermore, the S-glucuronidation of PTZ, followed by the rapid excretion, protects the conjugated sulfur atom against cleavage: the metabolite PTZ-desthio, that would result from the competing desulfuration reaction, was found systemically only to a very minor extent in the rat and goat metabolism studies (max. 0.5% of the dose in the bile and urine of the rat, similarly low amounts in compartments of the goat). PTZ-desthio was found at up to 18% in the faeces of the rat, but this portion was obviously formed locally in the intestine and was not absorbed in significant amounts.

In conclusion, owing to the sulfur atom, the S-glucuronidation is the unique metabolic principle of detoxification for PTZ in humans and mammals. The metabolite PTZ-desthio, containing a 1,2,4-triazole moiety, was found systemically only in trace amounts. Together with the aforementioned computational chemistry data, this unique metabolic behaviour completes the reasoning as to why exposure to PTZ does not cause the reproductive toxicity associated with classical triazoles and why PTZ has a generally very low toxicity in mammals.



6) References

- ¹ V. Morton, T. Staub, "A short history of fungicides", Online APSnet Features. **2008**, doi. 10.1094/APSnetFeature-2008-0306
- ² K.-H. Kuck, K. Stenzel, J.-P. Vors, „Sterol Biosynthesis Inhibitors.“ In: W. Krämer, U. Schirmer, P. Jeschke, M. Witschel (editors): Modern Crop Protection Compounds. Second edition, Wiley-VCH Verlag, Weinheim, Germany. **2012**, 761-805
- ³ J.A. Zarn, B.J. Bruschweiler, J.R. Schlatter, "Azole fungicides affect mammalian steroidogenesis by inhibiting sterol 14 alpha-demethylase and aromatase", Environ. Health Perspect. **2003**, 111(3): 255–61.
- ⁴ E.L. Schwartz, S. Hallam, R.E. Gallagher, P.H. Wiernik, "Inhibition of all-trans retinoic acid metabolism by fluconazole in vitro and in patients with acute promyelocytic leukemia", Biochem. Pharmacol. **1995**, 50(7): 923-928
- ⁵ C. Taxvig, U. Hass, M. Axelstad, M. Dalgaard, J. Boberg, H.R. Andersen, A.M. Vinggaard, "Endocrine-disrupting activities in vivo of the fungicides tebuconazole and epoxiconazole", Toxicol. Sci. **2007**, 100(2): 464-473
- ⁶ C. Taxvig, A.M Vinggaard., U. Hass, M. Axelstad, S. Metzдорff, C. Nelleman. "Endocrine disrupting properties in vivo of widely used azole fungicides", Int. J. Androl. **2008**, 31(2): 170-177;
- ⁷ G.M. Tiboni, F. Marotta, C. Rossi, F. Giampietro, "Effects of the aromatase inhibitor letrozole on in utero development in rats", Hum. Reprod. **2008**, 23(8): 1719-1723
- ⁸ S. Stinchcombe, S. Schneider, I. Fegert, M.C. Rey Moreno, V. Strauss, S. Gröters, E. Fabian, K.C. Fussell, G.H. Pigott, B. van Ravenzwaay, "Effects of estrogen co-administration on epoxiconazole toxicity in rats", Birth Defects Res. **2013**, 98: 247-259
- ⁹ M.C. Rey Moreno, K.C. Fussell, S. Gröters, S. Schneider, V. Strauss, S. Stinchcombe, I. Fegert, M. Versa, B. van Ravenzwaay, "Epoxiconazole-induced degeneration of rat placenta and the effects of estradiol supplementation", Birth Defects Res. (Part B) **2013**, 98: 208-221
- ¹⁰ G.M Tiboni., F. Marotta, A.P. Castigliero, C. Rossi, "Impact of estrogen replacement on letrozole-induced embryopathic effects", Hum. Reprod. **2009**, 24(11): 2688-2692
- ¹¹ T.J. Pursley, I.K. Blomquist, J. Abraham, H.F. Andersen, J.A. Bartley, "Fluconazole-induced congenital anomalies in three infants", Clin. Infect. Dis. **1996**, 22(2): 336-340
- ¹² G.M. Tiboni, F. Marotta, A. del Corso, F. Giampietro, "Defining critical periods for itraconazole-induced cleft palate, limb defects and axial skeletal malformations in the mouse", Toxicol. Letters **2006**, 167(1): 8-18
- ¹³ H.S. Buttar, J.H. Moffat, C. Bura, "Pregnancy outcome in ketoconazole-treated rats and mice", Teratology **1989**, 39: 444
- ¹⁴ V.C.S. Amaral, G. P. Nunes Jr., "Ketoconazole- and fluconazole-induced embryotoxicity and skeletal anomalies in Wistar rats: a comparative study", Braz. Arch. Biol. Technol. **2010**, 51(6): 1153-1161
- ¹⁵ E. Menegola, M.L. Broccia, F. Di Renzo, V. Massa, E. Giavini, "Craniofacial and axial skeletal defects induced by the fungicide triadimefon in the mouse", Birth Defects Res. (Part B) **2005**, 74(2): 185-195



-
- ¹⁶ B. Pilmis, V. Jullien, J. Sobel, M. Lecuit, O. Lotholary, C. Charlier, “*Antifungal drugs during pregnancy: an updated review*”, J. Antimicrob. Chemother. **2015**, 70(1): 14-22
- ¹⁷ M.M. Howley, T.C. Carter, M.L. Browne, P.A. Romitti, C.M. Cunnliff, C.M. Druschel, “*Fluconazole use and birth defects in the National Birth Defects Prevention Register*”, Am. J. Obstet. Gynecol. **2016**, 214(5): 657-658
- ¹⁸ E. Menegola, M.L. Broccia, F. Di Renzo, E. Giavini, “*Postulated pathogenic pathway in triazole fungicide-induced dysmorphogenetic effects*”, Reprod. Toxicol. **2006**, 22(2): 186-195
- ¹⁹ F. Marotta, G.M. Tibono, “*Molecular aspects of azoles-induced teratogenesis*”, Expert Opin. Drug Metab. Toxicol. **2010**, 6(4): 461-482
- ²⁰ M. Jautelat, H.-L. Elbe, J. Benet-Buchholz, W. Etzel, “*Chemistry of Prothioconazole (JAU6476)*”, Pflanzenschutz-Nachrichten Bayer **2004**, 57(2): 145-162
- ²¹ European Commission (2018): Draft (Renewal) Assessment Report prepared according to the Commission Regulation (EU) N° 1107/2009. PROTHIOCONAZOLE, Volume 3 – B.6 (AS). Rapporteur Member State : UK, Co-Rapporteur Member State : France. B.6.6. REPRODUCTIVE TOXICITY
- ²² L. Kjeldsen, M. Ghisari, E. Bonefeld-Joergensen, “*Currently used pesticides and their mixtures affect the function of sex hormone receptors and aromatase enzyme activity*”, Toxicol Appl Pharmacol **2013**, 272(2): 453-64
- ²³ J.E. Parker, A.G.S Warrilow, H.J. Cools, C.M. Martel, W.D. Nes, B.A. Fraaije, J.A. Lucas, D.E. Kelly, S.L. Kelly, “*Mechanism of binding of prothioconazole to Mycosphaerella graminicola CYP51 differs from that of other azole antifungals*”, Appl. Envir. Microbiol. **2011**, 77(4): 1460-1465
- ²⁴ A.G. Warrilow, J. E. Parker, D.E. Kelly, S.L. Kelly “*Azole Affinity of Sterol 14-Demethylase (CYP51) Enzymes from Candida albicans and Homo sapiens*”, Antimicrobial Agents Chemotherapy **2013**, 57(3): 1352-1360
- ²⁵ M. Dimopoulou, A. Verhoef, J.L.A. Pennings, B. van Ravenzwaay, I.M.C.M. Rietjens, A.H. Piersma. “*A transcriptomic approach for evaluating the relative potency and mechanism of action of azoles in the rat Whole Embryo Culture*”, Toxicology **2017**, 392: 96-105
- ²⁶ M. Dimopoulou, A. Verhoef, C.A. Gomes, C.W. van Dongen, I.M.C.M. Rietjens, A.H. Piersma, B. van Ravenzwaay. “*A comparison of the embryonic stem cell test and whole embryo culture assay combined with the BeWo placental passage model for predicting the embryotoxicity of azoles*”, Toxicology Letters **2018**, 286: 10-21
- ²⁷ M. Dimopoulou, A. Verhoef, J.L.A. Pennings, B. van Ravenzwaay, I.M.C.M. Rietjens, A.H. Piersma., “*Embryotoxic and pharmacologic potency ranking of six azoles in the rat whole embryo culture by morphological and transcriptomic analysis*”, Toxicol Appl Pharmacol. **2017**, 322: 15-26
- ²⁸ M. Haas, K. Justus, “*Metabolism of Prothioconazole (JAU6476) in animals and plants*”, Pflanzenschutz-Nachrichten Bayer **2004**, 57(2): 207-224.
- ²⁹ E. Hellpointer, H. Borchers, “*Behaviour of Prothioconazole (JAU6476) in the environment*”, Pflanzenschutz-Nachrichten Bayer **2004**, 57(2): 163-180.



- ³⁰ J. E. Parker, A. G. S. Warrilow, H. J. Cools, B. A. Fraaije, J. A. Lucas, K. Rigdova, W.J. Griffiths, D. E. Kelly, S. L. Kelly, "Prothioconazole and Prothioconazole-Desthio Activities against *Candida albicans* Sterol 14-Demethylase", *Appl. Environ. Microbiol.*, **2013**, 79(5): 1639–1645
- ³¹ J. D. A. Tyndall, M. Sabherwal, A. A. Sagatova, M. V. Keniya, J. Negroni, R. K. Wilson, M.A. Woods, K. Tietjen, B. C. Monk, "Structural and Functional Elucidation of Yeast Lanosterol 14 α -Demethylase in Complex with Agrochemical Antifungals", *PLoS ONE*, **2016**, 11(12): 1-18
- ³² Protein Data Bank; <https://www.rcsb.org/>
- ³³ D. Bohm, Y. Aharonov, „Discussion of Experimental Proof for the Paradox of Einstein, Rosen and Podolsky“, *Phys. Rev.* **1957**, 108: 1070
- ³⁴ W. Kohn, "Nobel Lecture: Electronic structure of matter – wave functions and density functionals", *Rev. Mod. Phys.* **1999**, 71: 1253-1266
- ³⁵ L Wang, Y. Wu, Y. Deng, B. Kim, L. Pierce, G. Krilov, D. Lupyán, Sh. Robinson, M.K. Dahlgren, J. Greenwood, D.L. Romero, C. Masse, J. L. Knight, Th. Steinbrecher, Th. Beuming, W. Damm, E. Harder, W. Sherman, M. Brewer, R. Wester, M. Murcko, L. Frye, R. Farid, T. Lin, D.L. Mobley, W.L. Jorgensen, B.J. Berne, R.A. Friesner, R. Abel, "Accurate and Reliable Prediction of Relative Ligand Binding Potency in Prospective Drug Discovery by Way of a Modern Free-Energy Calculation Protocol and Force Field", *J. Am. Chem. Soc.* **2015**, 137: 2695-2703
- ³⁶ J. C. Schöneboom, W. Thiel, „The Resting State of P450cam: A QM/MM Study“, *J. Phys. Chem. B* **2004**, 108: 7468-7478
- ³⁷ M. Sono, M. P. Roach, E.D. Coulter, J. H. Dawson, "Heme-Containing Oxygenases", *Chem. Rev.* **1996**, 96: 2841-2887
- ³⁸ A. Luthra, I. G. Denisov, S. G. Sligar, "Spectroscopic features of cytochrome P450 reaction intermediates", *Arch Biochem Biophys.* **2011**, 507(1): 26–35.
- ³⁹ P.R. Balding, C. S. Porro, K. J. McLean, M. J. Sutcliffe, J.-D. Marechal, A.W. Munro, S.P. de Visser, "How Do Azoles Inhibit Cytochrome P450 Enzymes? A Density Functional Study", *J. Phys. Chem. A* **2008**, 112: 12911–12918
- ⁴⁰ C.S. Poornima, P.M. Dean, "Hydration in drug design. 1. Multiple hydrogen-bonding features of water molecules in mediating protein-ligand interactions", *J. Comput. Aid. Mol. Design*, **1995**, 9: 500-512
- ⁴¹ A. D. Becke, "Density-functional exchange-energy approximation with correct asymptotic behavior", *Phys. Rev. A* **1988**, 38: 3098-3100
- ⁴² J.P. Perdew, "Density-functional approximation for the correlation energy of the inhomogeneous electron gas", *Phys. Rev. B* **1986**, 33: 8822-8824
- ⁴³ K. Jankowski, R. Becherer, P. Scharf, R. Ahlrichs, „The impact of higher polarization basis functions on molecular ab initio results. I. The ground state of F₂“, *J. Chem. Phys.* **1985**, 82: 1413–1419
- ⁴⁴ S. Grimme, J. Antony, S. Ehrlich, H. Krieg, „A consistent and accurate ab initio parametrization of density functional dispersion correction (DFT-D) for the 94 elements H-Pu“, *J. Chem. Phys.* **2010**, 132: 154104



-
- ⁴⁵ E. van Lenthe, J. G. Snijders, E. J. Baerends, "The zero-order regular approximation for relativistic effects: The effect of spin-orbit coupling in closed shell molecules", *J. Chem. Phys.* **1996**, 105 (15): 6505-6516
- ⁴⁶ F. Neese, "The ORCA program system". Wiley Interdisciplinary Reviews: Computational Molecular Science. **2012**, 2(1): 73–78
- ⁴⁷ F. Neese, "Software update: The ORCA program system, version 4.0". Wiley Interdisciplinary Reviews: Computational Molecular Science. **2018**, 8(1): 1327
- ⁴⁸ T. A. Keith, "AIMAll (Version 17.11.14)", TK Gristmill Software, Overland Park KS, USA, **2017** (aim.tkgristmill.com)
- ⁴⁹ Schrödinger Release 2018-1: Maestro, Schrödinger, LLC, New York, NY, **2018**.
- ⁵⁰ The very first such calculations were performed on the nicotinic acetyl cholin receptor, and were presented last year: M.E. Beck, "Digging deep into binding modes in protein-ligand-complexes by quantum chemistry", presented at the 11th Triennial Congress of the World Association of Theoretical and Computational Chemists (WATOC), Munich, **2017**. A manuscript is in preparation.
- ⁵¹ S. Raub, "Entwicklung einer Bewertungsfunktion für das Docking von Liganden in Proteine und artifizielle Rezeptoren", PhD thesis (Chapter 4), Heinrich-Heine-University, Düsseldorf, **2007**
- ⁵² N.C. Handy, private communication, **1996**
- ⁵³ R. Bader, "Atoms in Molecules: A Quantum Theory", **1994**, Oxford University Press, USA
- ⁵⁴ M.E. Beck, O. Gutbrod, S. Matthiessen, "Back Cover: Insight into the Binding Mode of Agonists of the Nicotinic Acetylcholine Receptor from Calculated Electron Densities", *ChemPhysChem* **2015**, 16: 2760 –2767
- ⁵⁵ M. Saitow, U. Becker, Ch. Riplinger, E.F. Valeev, F. Neese, "A new near-linear scaling, efficient and accurate, open-shell domain-based local pair natural orbital coupled cluster singles and doubles theory", *J. Chem. Phys.* **2017**, 146(16):164105
- ⁵⁶ [https://en.wikipedia.org/wiki/Enzyme#\"Lock_and_key\"_model](https://en.wikipedia.org/wiki/Enzyme#\)
- ⁵⁷ C. Helvig, M. Taimi, D. Cameron, G. Jones, M. Petkivich, "Functional properties and substrate characterization of human CYP26A1, CYP26B1, and CYP26C1 expressed by recombinant baculovirus in insect cells", *J. Pharmacol. Toxicol. Methods*, **2011**, 64(3): 258-263
- ⁵⁸ PDB IDs: 2VE3, 2VE4; K. Kühnel, N. Ke, M.J. Cryle, S.G. Sligar, M.A. Schuler, I. Schlichting, "Crystal structures of substrate free and retinoic acid bound cyanobacterial cytochrome P450 CYP120A1", *Biochem.*, 2008, 47(25): 6552-6559.
- ⁵⁹ B. Buttrick, "Characterization of selective and potent inhibitors of the human retinoic acid hydroxylases CYP26A1 and CYP26B1", master of science thesis **2012**, University of Washington, USA